J. Plasma Physics (2001), *vol.* 65, *part* 5, *pp.* 407–452.
DOI: 10.1017/S0022377801001246 Printed in the United Kingdom

Evaluating the efficiency of radiofrequency heating in tokamaks: the impact of orbital topology and poloidal inhomogeneity

DIRK VAN EESTER

Laboratorium voor Plasmafysica/Laboratoire de Physique des Plasmas, Associatie 'Euratom–Belgische Staat'/Association 'Euratom–Etat Belge', Koninklijke Militaire School/Ecole Royale Militaire, Trilateral Euregio Cluster, Brussels, Belgium

(Received 1 August 2000 and in revised form 3 November 2000)

Abstract. Radiofrequency heating in toroidal geometry is described. Starting from a general theory, expressions for the dielectric response and the radiofrequency diffusion operator are obtained. The computationally most efficient simplified expressions bear a close resemblance to the results of uniform plasma theory, but differ from them in their interpretation. In cases where the simplified expressions do not describe the physics faithfully, more general but computationally slower ones are available. Rigorously accounting for the geometry and the wave field yields fine structure that is commonly overlooked. Aside from causing the well-known $k_{\|}$-upshift or downshift impacting on the Doppler shift, the non-zero poloidal magnetic field modifies the orbital topology and forces one to account for the poloidal inhomogeneity of the static magnetic field. The expressions obtained restore intuition on how an electric field interacts with a charged particle, but, in so doing, cast doubt on the degree of realism of predictions of simplified models that do not account for the constructive or destructive interference phenomena introduced by the orbital topology non-uniformity. The expressions represent a numerical challenge, but show the necessity for the detailed description: the 'coarse-graining' underlying simplified models yields a result that has the right order of magnitude for interference related to crosstalk between resonances or multiple encounters with a given resonance, but may be an order of magnitude wrong for predictions on the combined effect of a poloidal mode spectrum. A Fokker–Planck code BATCH (Bounce-Averaged Tool for Cyclotron Heating), relying on the expressions obtained, is presented and some results are discussed.

1. Introduction

Modelling radiofrequency (RF) heating is usually done relying on a number of simplifying assumptions. Because of the widely differing time scales of the wave oscillations and the diffusion processes, and because the externally launched electric field energy is small compared with that contained in the static magnetic field, one can linearize the equations and separate the time scales. Although the resulting equations (the wave equation on the one hand and the Fokker–Planck equation on the other) describe different time scales, they are describing the same physics and are intimately connected: the average energy transferred from the waves to the

particles, when averaged over all fast processes as predicted by the wave equation solver, should be identical to the RF power density gain by the particles as computed by the Fokker–Planck solver. Unfortunately, the assumptions made to arrive at a wave equation and those adopted for deriving a Fokker–Planck equation are usually not the same. As a result, the question of consistency arises: How should one 'translate' the output of the wave equation code into the input for the Fokker–Planck code? One approximation that is often used is to compute the electric field structure with a wave code assuming thermodynamic equilibrium, and to adjust the magnitude of the field in the Fokker–Planck code to arrive at an integrated RF power density that equals the experimentally launched power (see e.g. Scharer et al. 1985; Hamamatsu et al. 1989). Another approach consists of adopting a simplified electric field, omitting details such as the local pattern and phase of the actual field (see e.g. O'Brien et al. (1986) and Kupfer (1991), in which the rudimentary wave description spoils an otherwise-sophisticated theory). Details such as the $k_{\|}$-upshift or downshift due to the finite poloidal magnetic field, the actual local wave phase or the fact that the cyclotron frequency varies along the orbit are thus – not always justifiably – omitted. Rather than accounting for the actual distribution (which is outside the scope of the Maxwellian plasma-wave code), one subsequently computes the average energy of the RF-heated distribution and modifies the temperature of the Maxwellian in the wave code to coincide with two-thirds of the obtained average energy. This procedure is then repeated until numerical convergence is reached. One may wonder if the result thus obtained reflects the actual physical situation. In view of the fact that the RF heating only takes place in the Doppler-shifted resonance region, can it, for example, be justified to assume that the RF heating is uniformly smeared out over a magnetic surface in the Fokker–Planck code? In view of the fact that harmonic heating preferentially acts on particles that already have a large perpendicular energy, is it meaningful to replace in the wave code the actual (highly non-isotropic) distribution by one that is isotropic?

To overcome the weaknesses of such crude (but numerically fast and therefore appealing) models, one should develop a model that places the wave and Fokker–Planck equations on the same footing. In such a model, the power launched from the antenna in the wave description is equal to the summed RF power densities on the various species as modelled by the Fokker–Plank description. In contrast to the previous procedure, no 'adjustment knob' exists to fine-tune the RF power densities of the two codes until they match. The skeleton of such a procedure was proposed long ago by Kaufman (1972). In his paper, Kaufman adopted the Hamiltonian action-angle technique to tackle the two-time-scale RF problem. After a coordinate transformation to the action-angle variables, solving the problem became straightforward. The appealingly simple formulae he proposed would, however, have to wait a long time before anyone actually started to use them, the reason being that a delicate part of the problem was not tackled in the paper, namely the evaluation of the Fourier spectrum of various quantities needed in the computation. As time passed, pieces of the puzzle were added one by one. Gambier and Samain (1985) made a first attempt to 'translate' Kaufman's formulae to more intuitive ones. Then Edery and Picq applied these results to write the ALCYON wave code in collaboration with Samain and Gambier (Edery and Picq 1986; Edery et al. 1987). Bécoulet et al. (1985, 1991) further refined the wave code. In spite of the tremendous potential of the action-angle method, no attempt was (at least to my knowledge) ever made to directly use the action-angle variables in

a wave code for non-Maxwellian distributions in a tokamak. Adopting the more intuitive trajectory integral method rather than that proposed by Kaufman, Lamalle (1993, 1997) started to look into the wave aspects of the problem addressed by Bécoulet et al. Because Kaufman showed how to devise a Fokker–Planck code in total agreement with the wave code, work on a Fokker–Planck code also relying on the trajectory method was initiated in parallel a little later (Van Eester 1995). Although based on the same physical assumptions and thus necessarily equivalent, the full equivalence of the trajectory method and the Hamiltonian approach was demonstrated only recently (Van Eester 1999). Parallel with the developments relying on the trajectory integral, Hedin et al. (1998, 1999) based themselves more directly on Kaufman's results to develop an equivalent approach to the same problem. Rather than solving the Fokker–Planck equation directly, they adopted the Monte Carlo approach to solve this equation by considering a large enough number of test particles to have good statistics on the distribution function (enough particles in each elementary box in configuration space) (Eriksson and Helander 1994; Eriksson et al. 1999). Whereas the trajectory integral method used by Lamalle and Van Eester expresses all quantities in terms of the constants of motion (c.o.m.) in the absence of the perturbed field, and thus expresses dielectric response as a function of these c.o.m., the results of the Monte Carlo approach are exploited to do the opposite. Translating the c.o.m. into local values of the parallel and perpendicular velocities of the particle, the local distribution is reconstructed and the local dielectric response, needed in the wave equation, evaluated. The advantage of this approach is that it can account for finite-banana-width effects without particular problems. The major drawback is that it takes many particles (and thus much computer time) to ensure a realistic statistical description. The presently existing numerical codes relying on the Monte Carlo approach further implicitly assume that decorrelation is sufficiently efficient to decouple resonances. Assuming that sufficient computer power is available to guarantee good statistics, one could envisage the addition of supplementary physics to refine this elegant description and test decorrelation from first principles. Various authors have pointed out that the large excursions of guiding-centre orbits from a magnetic surface have a non-negligible effect on the RF-heating performance (see e.g. Eriksson et al. 1993; Hellsten et al. 1995; Chang et al. 1999; and the previously mentioned Monte Carlo references). For the standard high-plasma-current experiments in ITER, their impact is expected to be marginal – but in low-plasma-current experiments, their impact is not a small physical effect. A rigorous treatment of effects such as RF-enhanced particle exhaust and plasma rotation critically involves adding neoclassical RF-induced radial transport to the Fokker–Planck equation – not only making the problem fully three-dimensional but also requiring that account be taken of competing transport mechanisms to make a reasonable prediction of the fate of RF-heated populations. These effects are beyond the scope of the work presented in the present paper.

The key to practically solving the RF problem in a self-consistent way relying on Kaufman's work is the evaluation of the Fourier spectrum of the RF-induced energy change. In view of the axisymmetry of the tokamak, and of the orthogonality of the gyro-modes, the only Fourier amplitudes that are hard to determine in practice are those of the bounce spectrum. Belikov and Kolesnichenko (1982, 1994) showed how this can be done relying on asymptotic techniques. They omitted, however, the role of the Doppler shift in their expressions. Adding the Doppler shift but

still relying on the same asymptotic techniques, relating nearby stationary-phase (SP) points and substituting the sum on the bounce modes for a bounce integral, yields expressions that are appealingly simple (see later): to lowest order in the drift parameter, they formally look like uniform plasma expressions, except that they have a phase factor stemming from the poloidal-mode-dependence of the field (which is what one would intuitively expect), and they need to be bounce-averaged (as has been standard in Fokker–Planck descriptions for many years). The price to pay for this simplicity is that the expressions obtained do not always faithfully describe the RF heating. The failure of the approximate expressions leads to the reappearance of an old problem even for a Maxwellian plasma, namely that positive-definite power absorption cannot be guaranteed analytically. The more general expressions do not suffer from this disadvantage, though, and should therefore be used.

In this paper, the practical implementation in a bounce-averaged Fokker–Planck code of both the simple and the more general expressions is discussed. A number of examples are given to illustrate how the present description differs from descriptions based implicitly on (quasi)uniform plasma expressions. A few preliminary examples of the Fokker–Planck code are also discussed. At present, the BATCH code is used as a stand-alone application. It either takes the electric field computed by the CYRANO wave code (Lamalle 1994, 1998) or simple analytical expressions for the field as input. The CYRANO code solves the wave equation for all three components of the electric field in tokamak geometry. It assumes Maxwellian distribution functions and allows one to describe waves absorbed by Landau, TTMP or fundamental cyclotron damping. Once CYRANO becomes able to solve the wave equation for non-Maxwellian distributions, the BATCH code will directly receive the RF diffusion coefficients from the CYRANO code (rather than evaluating them autonomously starting from the Fourier components of the field, as it does now), thus guaranteeing a fully self-consistent and as rapid as possible a description of the RF-heating process. The coupled wave plus Fokker–Planck equations can then be solved iteratively. As will be shown in this paper, the fine structure introduced when accounting for the tokamak geometry in a more rigorous way is not evidently resolved numerically. This is already a challenge for the Fokker–Planck code, which only needs to account for the active part of the dielectric response (related to the damping of the waves), and thus only needs information related to the resonant bounce mode. Since the wave code requires knowledge of the full bounce spectrum to evaluate the reactive part of the response (related to wave propagation), it represents an even more demanding challenge to describe the wave aspect of RF heating with a fair degree of realism. Further analytical work may yield acceptable approximations. The use of parallel computers may also help in tackling the problem.

This paper is structured as follows. First, the adopted quasilinear diffusion approach is sketched. After that, the computation of the orbit is discussed. This step yields expressions for the time history of the orbit. These expressions can be manipulated analytically, and make the computation of the bounce spectrum of the RF-induced energy change (the key ingredient in the dielectric response) less abstract. Illustrations are provided to show the strengths and weaknesses of various approaches. After that, the collision operator is briefly discussed and some comments on the adopted weak Galerkin method are given. Finally, a few examples of the Fokker–Planck code are provided, and conclusions are drawn.

2. Derivation of the wave equation and quasilinear diffusion operator

The basic equations describing RF heating relying on the trajectory integral method have been discussed in detail elsewhere (see e.g. Van Eester 1995, 1998, 1999; and references therein), and will be discussed only briefly here. The standard quasilinear approach is adopted, and only leading-order contributions in the drift parameter are considered (i.e. guiding-centre orbits are confined to magnetic surfaces). The starting point is the evolution equation of the distribution function:

$$\frac{dF}{dt} = \left.\frac{\partial F}{\partial t}\right|_{\text{slow}}.$$

The total time derivative on the left-hand side is evaluated along the particle trajectory, and the operator acting on the distribution on the right-hand side of the equation represents Coulomb collisions as well as particle gains and losses. Realizing that two time scales are involved in the heating process, one splits the distribution into two parts:

$$F = F_0(\mathbf{\Lambda}, t_{\text{slow}}) + f_{RF}(\mathbf{\Lambda}, \mathbf{\Phi}, t_{\text{fast}}).$$

The first part is slowly varying, i.e. it depends only on a 'slow' time and on the variables $\mathbf{\Lambda}$ that are c.o.m. in the absence of the RF perturbation. The second part depends on the c.o.m. variables $\mathbf{\Lambda}$ as well as on the angles $\mathbf{\Phi}$ parametrizing the periodic and fast bounce, gyro, and toroidal drift aspects of the motion. It varies on a rapid time scale, but has an amplitude that is small with respect to the slowly varying distribution. The assumed smallness of the electromagnetic field with respect to the static magnetic field and of f_{RF} with respect to the slowly varying distribution function allows one to introduce an ordering in the evolution equation. The static magnetic field imposes the charged particles' orbits; these orbits are perturbed by the time-dependent electromagnetic field. When the perturbing field oscillates at the generator frequency ω, one can write

$$\mathbf{E} = \mathbf{E}_{RF}(\mathbf{x}, t_{\text{fast}}),$$

$$\mathbf{B} = \mathbf{B}_0(\mathbf{x}) + \mathbf{B}_{RF}(\mathbf{x}, t_{\text{fast}}),$$

$$\mathbf{E}_{RF}, \mathbf{B}_{RF}, f_{RF} \propto \exp(-i\omega t).$$

Introducing the above into the evolution equation yields (i) contributions of order 1, (ii) linear but rapidly varying terms and (iii) terms of second order in the linear quantities. Averaging over all 'fast' processes (bounce, drift and gyro motion, as well as driven temporal response) removes the linear but not the quadratic term in the evolution equation. The linear equation allows one to express the perturbed distribution in terms of F_0. This result is re-inserted into the original equation and the average is performed. The result is

$$\frac{\partial F_0}{\partial t} = \left.\frac{\partial F_0}{\partial t}\right|_{RF} + \text{slow processes}, \qquad f_{RF} = -\int^t dt'\, \mathbf{a}_{RF} \cdot \boldsymbol{\nabla}_{\mathbf{v}} F_0, \tag{1a,b}$$

$$\left.\frac{\partial F_0}{\partial t}\right|_{RF} = \frac{1}{2}\,\text{Re}\left\{\langle \boldsymbol{\nabla}_{\mathbf{v}} \cdot \mathbf{a}^*_{RF} \int^t dt'\, \mathbf{a}_{RF} \cdot \boldsymbol{\nabla}_{\mathbf{v}} \rangle F_0\right\}, \qquad \mathbf{a}_{RF} = \frac{q_s}{m_s}(\mathbf{E}_{RF} + \mathbf{v} \times \mathbf{B}_{RF}), \tag{1c,d}$$

$$\mathbf{a}_{RF} \cdot \boldsymbol{\nabla}_{\mathbf{v}} \Lambda_i = \left.\dot{\Lambda}_i\right|_{RF}. \tag{1e}$$

https://doi.org/10.1017/S0022377801001246 Published online by Cambridge University Press

Here the angular brackets $\langle\ \rangle$ indicate the average over $\mathbf{\Phi}$ and t_{fast}, and the 'overdot' ($\dot{}$) indicates the RF-induced temporal derivative along the unperturbed orbit, i.e. the orbit imposed by the zeroth-order magnetic field. Later in this paper, the subscript '*RF*' will be dropped whenever there is no ambiguity. The particular choice of the independent variables $\mathbf{\Lambda}$ and $\mathbf{\Phi}$ has great bearing on the algebraic complexity of the computations. When c.o.m. are adopted as three of the variables $\mathbf{\Lambda}$ (as is done here), the distribution function can, for example, be moved out of the trajectory integral in the above expressions. Following Kaufman's suggestion, one may further adopt the angles introduced in the action-angle formalism. These angles vary linearly with time and thus greatly facilitate the evaluation of the trajectory integral. The relation between these angles and the usual ones is given by

$$\theta = \text{const}_{tp}\Phi_b + \text{periodic function}(\Phi_b),$$

$$\varphi = \Phi_d + \text{periodic function}(\Phi_b),$$

$$\phi = \Phi_b + \text{periodic function}(\Phi_b).$$

For passing particles, the angle Φ_b is unique. For trapped particles, the angle Φ_b can be taken to be either the 'bounce angle' (varying from 0 to 2π in a complete bounce including the co- and the counter-rotating parts of the orbit) or the 'transit angle' (varying by 2π in between the two banana tips $\theta_{\min}$ and $\theta_{\max}$, i.e. splitting the trapped particle orbit in two and treating the trapped particle as the 'sum' of two passing particles, for which part of the magnetic surface is excluded but which feel the same collisional drag). The former definition links Φ_b to time via the bounce frequency, but does not allow a 1-to-1 correspondence between the poloidal angle θ and the angle Φ_b; for this choice const_{tp} is 1 for passing and 0 for trapped particles. The latter definition introduces the transit rather than the bounce frequency but allows a 1-to-1 θ–Φ_b correspondence; for this choice const_{tp} is 1 for the passing and the $(\theta_{\max} - \theta_{\min})/2\pi$ for trapped particles. Note that, because the equilibrium does not depend on the toroidal angle φ or on the gyroangle ϕ,

$$\frac{\partial}{\partial \Phi_g} = \frac{\partial}{\partial \phi}, \qquad \frac{\partial}{\partial \Phi_d} = \frac{\partial}{\partial \varphi}.$$

The perturbed distribution function also appears in the RF-perturbed current density in the wave equation:

$$\boldsymbol{\nabla} \times \boldsymbol{\nabla} \times \mathbf{E} - k_0^2 \mathbf{E} = i\omega\mu_0 \left[\mathbf{J}_{\text{antenna}} - \sum_{\text{species } s} q \int d\mathbf{v} \int^t dt' \frac{q_s}{m_s} \left(\mathbf{E} + \frac{\mathbf{v} \times \boldsymbol{\nabla} \times \mathbf{E}}{i\omega} \right) \cdot \boldsymbol{\nabla}_{\mathbf{v}} F_0 \right]. \quad (2)$$

To guarantee a fully self-consistent description of RF heating, the interaction between particles and waves can be analysed in terms of individual guiding-centre-orbit contributions ('building blocks'), which are independent of the distribution function, and which are used both in the wave and Fokker–Planck solvers. When adopting such elementary 'building blocks', changing the level of sophistication with which the particle–wave interaction is described only requires changing these blocks while leaving the rest of the numerical model untouched.

https://doi.org/10.1017/S0022377801001246 Published online by Cambridge University Press

Using the identity

$$\mathbf{E}+\mathbf{v}\times\mathbf{B}=\frac{i}{\omega}\left(\frac{d}{dt}\boldsymbol{\nabla}_{\mathbf{v}}-\boldsymbol{\nabla}_{\mathbf{x}}\right)\mathbf{E}\cdot\mathbf{v},$$

the RF-induced time derivative of the c.o.m. $\boldsymbol{\Lambda}$ can be computed. Depending on the variables $\boldsymbol{\Lambda}$ chosen, slightly different results are found. If the energy ε, the magnetic moment μ and the toroidal angular momentum P are the adopted $\boldsymbol{\Lambda}$, one readily finds

$$\boldsymbol{\Lambda}=\left(\varepsilon=\tfrac{1}{2}m_s v^2,\quad \mu=m_s\frac{v_\perp^2}{2B_0},\quad P=\Psi-\frac{2\pi m_s R v_\varphi}{q_s}\right),$$

$$\dot{\boldsymbol{\Lambda}}=\frac{q}{m}(\mathbf{E}+\mathbf{v}\times\mathbf{B})\cdot\boldsymbol{\nabla}_{\mathbf{v}}\boldsymbol{\Lambda}=-\sum_{\mathbf{m}}\dot{\varepsilon}_m\frac{\mathbf{h}_{\mathbf{m}}}{\omega}+\frac{d}{dt}(\ldots),$$

$$\dot{\varepsilon}=\frac{q}{m}(\mathbf{E}+\mathbf{v}\times\mathbf{B})\cdot\boldsymbol{\nabla}_{\mathbf{v}}\varepsilon=q\mathbf{E}\cdot\mathbf{v}=\sum_{\mathbf{m}}\dot{\varepsilon}_{\mathbf{m}}e^{i\mathbf{m}\cdot\boldsymbol{\Phi}},$$

$$\dot{\varepsilon}_{\mathbf{m}}=\frac{1}{(2\pi)^3}\int_0^{2\pi}d\boldsymbol{\Phi}\,q\mathbf{E}\cdot\mathbf{v}e^{-i\mathbf{m}\cdot\boldsymbol{\Phi}},$$

$$\mathbf{h}_{\mathbf{m}}=(-\omega,m_d,m_g),$$

in which $\mathbf{m}$ is the vector of mode numbers m_b, m_d and m_g with reference to the angles $\boldsymbol{\Phi}=(\Phi_b,\Phi_d,\Phi_g)$. Again the 'overdot' ($\dot{}$) indicates the RF-induced time derivative along the unperturbed orbit. The corresponding quasilinear diffusion operator is

$$\begin{aligned}Q=\frac{1}{2}\mathrm{Re}\Bigg\{&\frac{1}{J}\begin{pmatrix}\frac{\partial}{\partial\varepsilon} & \frac{\partial}{\partial\mu} & \frac{\partial}{\partial P}\end{pmatrix}J\\&\times\begin{pmatrix}\left\langle\dot{\varepsilon}^*\int_{-\infty}^t dt'\,\dot{\varepsilon}\right\rangle & \left\langle\dot{\varepsilon}^*\int_{-\infty}^t dt'\,\dot{\mu}\right\rangle & \left\langle\dot{\varepsilon}^*\int_{-\infty}^t dt'\,\dot{P}\right\rangle\\ \left\langle\dot{\mu}^*\int_{-\infty}^t dt'\,\dot{\varepsilon}\right\rangle & \left\langle\dot{\mu}^*\int_{-\infty}^t dt'\,\dot{\mu}\right\rangle & \left\langle\dot{\mu}^*\int_{-\infty}^t dt'\,\dot{P}\right\rangle\\ \left\langle\dot{P}^*\int_{-\infty}^t dt'\,\dot{\varepsilon}\right\rangle & \left\langle\dot{P}^*\int_{-\infty}^t dt'\,\dot{\mu}\right\rangle & \left\langle\dot{P}^*\int_{-\infty}^t dt'\,\dot{P}\right\rangle\end{pmatrix}\begin{pmatrix}\frac{\partial}{\partial\varepsilon}\\ \frac{\partial}{\partial\mu}\\ \frac{\partial}{\partial P}\end{pmatrix}\Bigg\}\\=\sum_{\mathbf{m}}\sum_{\mathbf{m}'}\frac{1}{2}\mathrm{Re}\Bigg\{&\frac{1}{J}\begin{pmatrix}\frac{\partial}{\partial\varepsilon} & \frac{\partial}{\partial\mu} & \frac{\partial}{\partial P}\end{pmatrix}\cdot\mathbf{h}^*_{\mathbf{m}'}J\left\langle\dot{\varepsilon}^*_{\mathbf{m}'}e^{-i\mathbf{m}'\cdot\boldsymbol{\Phi}+\omega t}\right.\\&\left.\times\int_{-\infty}^t dt'\dot{\varepsilon}_{\mathbf{m}}\,e^{i\mathbf{m}\cdot\boldsymbol{\Phi}(t')-\omega t'}\right\rangle\mathbf{h}_{\mathbf{m}}\cdot\begin{pmatrix}\frac{\partial}{\partial\varepsilon}\\ \frac{\partial}{\partial\mu}\\ \frac{\partial}{\partial P}\end{pmatrix}\Bigg\}.\end{aligned}\tag{3}$$

https://doi.org/10.1017/S0022377801001246 Published online by Cambridge University Press

When the action-angle variables are preferred, the vector $\mathbf{h_m}$ is simply identical to the vector $\mathbf{m}$. Adopting the simplest possible decorrelation model ($\omega \rightarrow \omega + i\nu$), the integrals in the above reduce to

$$\sum_{\mathbf{m}}\sum_{\mathbf{m}'} \mathbf{h}^*_{\mathbf{m}'} \left\langle \dot{\varepsilon}^*_{\mathbf{m}'} e^{-i\mathbf{m}'\cdot\mathbf{\Phi}+\omega t} \int_{-\infty}^{t} dt' \dot{\varepsilon}_{\mathbf{m}} e^{-i\mathbf{m}\cdot\mathbf{\Phi}(t')-\omega t'} \right\rangle \mathbf{h_m} = \sum_{\mathbf{m}} \mathbf{h}^*_{\mathbf{m}} \frac{|\dot{\varepsilon}_{\mathbf{m}}|^2}{i(\mathbf{m}\cdot\boldsymbol{\omega}-\omega)} \mathbf{h_m}. \tag{4}$$

In this paper, and anticipating the coupling to the CYRANO wave code, the Fokker–Planck equation for the slowly varying distribution function F_0 will henceforth be written in terms of the particular constants of motion proposed in Lamalle (1997): the velocity v and the normalized magnetic moment $x = \mu B_{\scriptscriptstyle m}/\varepsilon$. Details on the adopted up–down-symmetric D-shaped equilibrium can be found in Appendix A. The Fokker–Planck equation is solved on the flux surface characterized by the radial coordinate ρ (= r for a circular plasma) on which the guiding centres lie. In the above, $B_{\scriptscriptstyle m}$ is the strength of the static magnetic field at some reference position. The specific choice for which the reference major-radius position corresponds to the low-field-side intersection of the guiding-centre orbit with the midplane ensures that x takes values between 0 and 1. This choice will be made henceforth. In the absence of auxiliary heating, the first variable v is a true constant of the motion on the rapid time scales on which the bounce, toroidal drift and gyro motions take place. To leading order in the drift parameter, the magnetic moment evaluated at the guiding-centre position and thus x are also invariants. Similarly, the guiding-centre trajectories are assumed to be confined to magnetic surfaces, i.e. the toroidal angular momentum P is reduced to the poloidal flux function Ψ, which only depends on the flux surface labelling parameter ρ. The replacement of P by Ψ is *not* without consequence: since the guiding centre makes *radial* excursions on a poloidal bounce, Ψ is not a true constant of the motion on the rapid time scales over which the Fokker–Planck equation is to be averaged. Consequently, $P \rightarrow \Psi$ implies that the RF-induced radial transport is no longer faithfully described: whereas classical RF-induced diffusion due to the gyro motion can be included by considering the full three-dimensional Fokker–Planck equation in (v, x, ρ) space, neoclassical effects on radial transport are currently not yet included in the model presented here, although they are formally included in Kaufman's original theory.

The distribution function F_0 depends on the variables $\mathbf{\Lambda} = (v, x, \rho)$, but not on the coordinates $\mathbf{\Phi} = (\Phi_b, \Phi_d, \Phi_g)$ parametrizing the fast but periodic bounce, toroidal drift and cyclotron motions respectively. All traces of the fast aspects of the motion are removed from the quasilinear equation by averaging its coefficients over the period motion $\mathbf{\Phi}$ and (fast) time. These averages are trivial when adopting $\mathbf{\Phi}$ angles that vary linearly with time such that $d\mathbf{\Phi}/dt = \boldsymbol{\omega}$ in which the frequencies $\boldsymbol{\omega} = (\omega_b, \omega_d, \omega_g)$ depend only on $\mathbf{\Lambda}$. The determination of the $\mathbf{\Phi}$-Fourier spectrum of the coefficients, needed to perform the averaging, will be discussed later. To leading order in the drift parameter, the Jacobian of the transformation $(\mathbf{x}, \mathbf{v}) \rightarrow (\mathbf{\Lambda}, \mathbf{\Phi})$ is

$$J = J_{\mathbf{\Lambda\Phi}} = \frac{d\Psi}{d\rho} \frac{v^3}{4\pi\omega_b B_{\scriptscriptstyle m}}, \tag{5}$$

in which ω_b is the poloidal transit frequency (ω_b is the bounce frequency for passing and twice that for trapped particles). The Fokker–Planck equation,

$$\frac{\partial}{\partial t} F_0 = (\mathscr{D} + \mathscr{C} - \mathscr{L}) F_0 + S, \tag{6}$$

https://doi.org/10.1017/S0022377801001246 Published online by Cambridge University Press

is solved using the weak form of the Galerkin formalism. In the above, $\mathscr{Q}$ and $\mathscr{C}$ are the RF and Coulomb collision operators while $\mathscr{L}$ represents the losses and S the sources. The Fokker–Planck equation is multiplied by a sufficiently smooth test function G and integrated by parts. The quasilinear term in the functional is of the form

$$\begin{aligned}\tilde{\mathscr{Q}}(G,F_0) &= \int d\mathbf{\Lambda}\, JG\mathscr{Q}F_0 \\ &= \int d\mathbf{\Lambda}\, JG\frac{1}{J}\begin{pmatrix}\dfrac{\partial}{\partial v} & \dfrac{\partial}{\partial x}\end{pmatrix} J\sum_N \frac{\mathscr{B}_N}{v^2}\begin{pmatrix}1 & \eta_N \\ \eta_N & \eta_N^2\end{pmatrix}\begin{pmatrix}\dfrac{\partial}{\partial v} \\ \dfrac{\partial}{\partial x}\end{pmatrix} F_0 \\ &= -\int d\mathbf{\Lambda}\, J\sum_N \mathscr{B}_N h_N(G)h_N(F_0) + \text{surface terms}, \end{aligned} \tag{7}$$

in which the last expression was obtained by partial integration to reduce the second-order differential operators acting on the distribution to first-order ones. Here $\mathscr{B}_N$ describes the interaction of the rapidly varying electric field

$$\mathbf{E} = \sum_n \sum_m \mathbf{E}_{mn}(\rho)\, \exp[i(m\theta + n\varphi - \omega t)]$$

with the orbit characterized by $\mathbf{\Lambda}$,

$$\eta_N = \frac{2(-x + N\Omega_m/\omega)}{v}$$

and N is the cyclotron harmonic number. The poloidal and toroidal angles are θ and φ, and their respective mode numbers are m and n. $\mathscr{B}_N$ contains the bounce-spectrum information from the multiple integral in (4):

$$\mathscr{B}_N = \mathrm{Re}\left\{\frac{1}{m_s^2}\sum_{m_b}\frac{|\hat{\varepsilon}_{\mathbf{m}}|^2}{i(\mathbf{m}\cdot\boldsymbol{\omega} - \omega)}\right\} \tag{8}$$

(the change of variable from the energy to the velocity brings out the factor m_s^{-2} in the partial derivatives to the left and right of the integral) and h_N is the differential operator

$$h_N(\cdot) = -\frac{1}{v}\left[\frac{\partial(\cdot)}{\partial v} + \eta_N\frac{\partial(\cdot)}{\partial x}\right]. \tag{9a}$$

The computation of the building blocks $\mathscr{B}_N$ is discussed in the next section. The differential operator h_N in the quasilinear term can locally along the guiding-centre orbit be expressed in the more familiar form (see e.g. Kennel and Engelman 1966)

$$h_N(\cdot) = \left(1 - \frac{k_\parallel v_\parallel}{\omega}\right)\frac{1}{v_\perp}\frac{\partial(\cdot)}{\partial v_\perp} + \frac{k_\parallel}{\omega}\frac{\partial(\cdot)}{\partial v_\parallel}, \tag{9b}$$

in which the variables should be evaluated at the local poloidal angle at which the resonance condition is satisfied. Note that the trapped/passing edge is at the constant normalized magnetic moment $x = \Omega_m/\Omega(\pi)$ and the tangent resonance at the banana tip is at the constant $x = N\Omega_m/\omega$. More generally, the resonance is at

$$x_{\mathrm{res}} = \frac{B_m}{B_0}\left[1 - \left(\frac{\omega - N\Omega_m B_0/B_m}{k_\parallel v}\right)^2\right],$$

https://doi.org/10.1017/S0022377801001246 Published online by Cambridge University Press

and the value of the parallel velocity at resonance is

$$v_{\|\mathrm{res}} = \frac{\omega - N\Omega_m B_0/B_m}{k_\|}.$$

After having computed the building blocks $\mathscr{B}_N$, all coefficients appearing in the Fokker–Planck equation (6) can be assembled and the equation can be directly solved numerically (see further). The variables adopted in this paper were proposed by Lamalle when studying the wave-equation counterpart of the description presented here; adopting other independent variables merely requires one to replace the differential operators and the Jacobian by those corresponding to the new ones. The weak Galerkin form of the wave equation is

$$\int d\mathbf{x}\, \frac{1}{i\omega\mu_0}(\boldsymbol{\nabla}\times\mathbf{F}^*\cdot\boldsymbol{\nabla}\times\mathbf{E}_{RF} - k_0\mathbf{F}^*\cdot\mathbf{E}_{RF})$$

$$= \int d\mathbf{S}\cdot\frac{\mathbf{F}^*\times\mathbf{B}_{RF}}{\mu_0} + \int d\mathbf{x}\ \mathbf{F}^*\cdot(\mathbf{J}_{RF}+\mathbf{J}_{\mathrm{antenna}}), \qquad (10)$$

$$\mathbf{J}_{RF} = \sum_s q_s \int d\mathbf{v}\ \mathbf{v} f_{RF},$$

in which $\mathbf{F}$ is a sufficiently smooth test-function vector. For the particular case of Maxwellian plasmas, an expression for the wave equation was obtained in Galerkin form for a toroidally curved but otherwise one-dimensional slab. In this equation, finite-Larmor-radius effects can be accounted for in principle up to any desired order, but to have practical expressions one relies on the assumption that the electric field's phase does not vary significantly on a Larmor radius requiring an a posteriori check of the wave field obtained when solving the wave code to ensure that the solution does not violate this basic assumption (and thereby to ensure that it is physically relevant). This is the weakness of all mode-conversion models based on a truncated finite-Larmor-radius series: if power is for example still carried by the ion Bernstein wave away from its conversion point with the fast wave, the predicted wave behaviour of this short-wavelength branch is doubtful at best. The only rigorous way to properly predict the wave behaviour of short-wavelength branches is to solve the integro-differential equation. The latter was done for example, by Sauter and Václavík (1992) for slab geometry and recently by Jaeger et al. (2000) for two-dimensional geometry. The TOMCAT (toroidal mode conversion and absorption tool) code solves the above wave equation, retaining terms up to second-order finite-Larmor-radius terms in the operator acting on the electric field and on the test function. The resulting system guarantees positive-definite absorption for both long- and short-wavelength branches up to the third harmonic (Van Eester and Koch 1998). The adopted method is equivalent to that proposed by Colestock and Kashuba (1983), but carried out further to consistently contain all second-order finite-Larmor-radius terms in the differential operator in the variational form of the wave equation rather than keeping only the dominant terms for each cyclotron harmonic. It is more common to truncate the dielectric response (rather than the operator acting on the field and the test function) at second-order finite-Larmor-radius terms (see e.g. Brambilla 1999). Such a truncation cannot guarantee positivity of the absorbed power when short-wavelength modes, which violate the basic assumption, are excited.

The surface terms in (7) correspond to the fluxes associated with the quantity G. For $G \equiv 1$, they represent the physical particle fluxes flowing from one finite element into the neighbouring ones. Because the physical flux is continuous, the numerical continuity of the surface terms is ensured by a choice of sufficiently smooth base functions. Provided that such an appropriate choice is made, these terms do not appear explicitly in the global linear system. They do, however, contribute to the *local* power and particle balance, so they have to be included when computing, for example, the RF-induced power density in a given finite element. Identifying G with the energy and integrating over the angles $\mathbf{\Phi}$, the total power absorption by all particles whose guiding centres are confined between two magnetic surfaces is obtained:

$$P_{\text{abs}} = \int d\mathbf{x}\, d\mathbf{v}\, \frac{mv^2}{2} \mathscr{Q} F_0 = -\sum_N (2\pi)^3 \int d\mathbf{\Lambda}\, J\, \mathscr{B}_N h_N \left(\frac{1}{2}mv^2\right) h_N(F_0)$$

$$= \sum_N (2\pi)^3 m_s \int d\mathbf{\Lambda}\, J \mathscr{B}_N h_N(F_0) = \frac{1}{2}\,\text{Re}\left\{\int d\mathbf{x}\, \mathbf{E}^* \cdot \mathbf{J}_{RFs}\right\}. \tag{11}$$

The functions $\mathscr{B}_N$ shared by the wave and Fokker–Planck equations guarantee a fully self-consistent treatment of the RF heating.

3. Computation of the orbits and related quantities

Prior to evaluating the building blocks, it is necesssary to compute the orbits. We start from the general expressions for the time derivative of the poloidal angle (for details on geometric quantities, the reader is referred to Appendix A), the toroidal angle and the gyrophase:

$$\dot{\theta} = \frac{d\theta}{dt} = \frac{v_\parallel \sin\,\alpha}{|\partial \mathbf{x}/\partial\theta|} = v \frac{\sin\,\alpha}{|\partial \mathbf{x}/\partial\theta|}\,\text{sign}(v_\parallel)\left(1 - \frac{xB_0}{B_m}\right)^{1/2}, \tag{12a}$$

$$\dot{\varphi} = \frac{d\varphi}{dt} = \frac{v_\parallel \cos\,\alpha}{R}, \tag{12b}$$

$$\dot{\phi} = \frac{d\phi}{dt} \approx -\mathbf{\Omega} = -\frac{q_s B_0}{m_s}, \tag{12c}$$

in which α is the angle between the toroidal and parallel directions. Removing all velocity dependence from the right-hand side of (12a), one arrives at the evolution equation for the time that it takes for a guiding centre with $v = 1\,\text{m}\,\text{s}^{-1}$ and $\text{sign}(v_\parallel^*) = 1$ to arrive at the poloidal position θ:

$$\frac{dt}{d\tilde{\theta}} = \frac{dt}{d[\theta/v\ \text{sign}(v_\parallel)]} = \frac{|\partial \mathbf{x}/\partial\theta|}{\sin\,\alpha(1 - xB_0/B_m)^{1/2}}.$$

In view of the fact that finite-banana-width effects are neglected (only leading-order terms in the drift parameter are kept), the above differential equation has to be solved numerically only once for a given x, and yields the evolution for any v and sign $(v_\parallel)$ by multiplying by the factor v sign $(v_\parallel)$. The integration is performed from the equatorial plane to π for passing particles. For trapped particles, the denominator becomes zero at the banana tip $\theta_{\max}$. Except at the trapped/passing edge, the integral is well behaved, however, and so one can find a good approximation to $t(\theta_{\max})$ by stopping the integration very close to but not at the banana tip (see

https://doi.org/10.1017/S0022377801001246 Published online by Cambridge University Press

Appendix B, which provides analytical expressions for the special case of a circular cross-section, for which all relevant quantities can be expressed in terms of elliptic functions). Once $t(\theta)$ has been determined numerically, one readily finds the Fourier spectrum $\mathscr{P}_l, \mathscr{T}_l$ and $\mathscr{G}_l$ of $d\theta(\Phi_b)/dt = d\theta(\omega_b t)/dt$, $d\varphi(\Phi_b)/dt$ and $d\phi(\Phi_b)/dt$ for $v(\mathrm{m\,s^{-1}} = \mathrm{sign}(v_\parallel) = 1$ relying on the fast Fourier technique. Once the Fourier spectrum is known, one can analytically determine $\theta(\Phi_b), \varphi(\Phi_b)$ and $\phi(\Phi_b)$:

$$\theta = \mathrm{sign}(v_\parallel) \left[\frac{\mathscr{P}_0}{\omega_b/v} \Phi_b + \sum_{l=1} \frac{\mathscr{P}_l}{l\omega_b/v} \sin(l\Phi_b) \right], \tag{13a}$$

$$\varphi = \mathrm{sign}(v_\parallel) \left[\frac{\mathscr{T}_0}{\omega_b/v} \Phi_b + \sum_{l=1} \frac{\mathscr{T}_l}{l\omega_b/v} \sin(l\Phi_b) \right], \tag{13b}$$

$$\phi = \frac{1}{v} \left[\frac{\mathscr{G}_0}{\omega_b/v} \Phi_b + \sum_{l=1} \frac{\mathscr{G}_l}{l\omega_b/v} \sin(l\Phi_b) \right], \tag{13c}$$

as well as any required derivative of these angles for any v and sign $(v_\parallel)$. In the above, the transit frequency ω_b was chosen always to be positive: Φ_b always grows with time, while θ may decrease or increase for advancing t. The transit frequency, toroidal drift frequency and (averaged) gyrofrequency can be found in the above:

$$\omega_b = \frac{\pi}{\theta_{\max}} v\mathscr{P}_0, \tag{14a}$$

$$\omega_d = \mathrm{sign}(v_\parallel)\, v\mathscr{T}_0, \tag{14b}$$

$$\omega_g = \mathscr{G}_0. \tag{14c}$$

The factor $\pi/\theta_{\max}$ in (14a) reminds us of the fact that we have split the trapped orbits in two and formally treat these orbits as a sum of two passing orbits belonging to particles for which part of the magnetic circumference is excluded. One orbit contains the history of the trapped particle between $\theta_{\min}$ and $\theta_{\max}$, and the other the history between $\theta_{\max}$ and $\theta_{\min}$. For the particular D-shaped equilibrium chosen here, up–down symmetry is assumed (see Appendix A), and $\theta_{\min} = -\theta_{\max}$. The angle Φ_b varies by 2π in both cases. The phase factor of the RF-induced energy change associated with the poloidal mode number m, the toroidal mode number n and the gyro mode number N is of the form

$$\Xi(\Phi_b) = m\theta + n\varphi - N\phi = \xi_0 \Phi_b + \sum_{l=1} \xi_l \sin(l\Phi_b), \tag{15}$$

the first term in which varies linearly with time while the others result from the poloidal *non*-uniformity of the static magnetic field.

4. Computation of the building blocks $\mathscr{B}_N$

In this section, the practical computation of the functions $\mathscr{B}_N$ is discussed. More details on the form of the RF diffusion operator and a short discussion of its connection to more familiar ones can be found in Van Eester (1995, 1998, 1999). Relying on causality, i.e. assuming the driver frequency to have a vanishingly small but

https://doi.org/10.1017/S0022377801001246 Published online by Cambridge University Press

positive imaginary part, the most general expression for the desired term is

$$\mathscr{B}_N = \mathrm{Re}\left\{\frac{1}{m_s^2}\sum_{m_b}\frac{|\dot{\varepsilon}_{\mathbf{m}}|^2}{i(\mathbf{m}\cdot\boldsymbol{\omega}-\omega)}\right\} = \frac{\pi}{m_s^2}|\dot{\varepsilon}_{(m_b,n,-N)}|^2\frac{\delta(m_b-[\omega-n\omega_d+N\omega_g]/\omega_b)}{\omega_b}$$
$$= \frac{\pi}{m_s^2}|\dot{\varepsilon}_{(m_b,n,-N)}|^2\frac{\delta(m_b-m_{b_{\mathrm{res}}})}{\omega_b}, \tag{16}$$

in which $\dot{\varepsilon}_{\mathbf{m}}$ is the Fourier amplitude of the RF-induced energy time derivative.

The evaluation of this amplitude is immediate for the drift and gyro-angles Φ_d and Φ_g, but owing to poloidal inhomogeneity the bounce integral is more cumbersome. Various methods have been proposed to evaluate this integral:

(i) Semi-analytical integration by first taking a fast Fourier transform of the guiding-centre motion, and subsequently performing the bounce integral analytically;

(ii) directly adopting the fast Fourier transform method to the full integral;

(iii) making use of the stationary-phase method.

The first method has the advantage that the bounce integrals are evaluated analytically without approximations, but requires bookkeeping of Bessel function indices; the abbreviation 'SA' will be adopted henceforth when referring to this semi-analytical method. It is most useful if the guiding-centre motion is well represented by a few Fourier components (limited phase variations per bounce).

The second method hinges on the integrand of the bounce integral to be well described by a limited number of Fourier modes, and is thus also most useful when the phase varies little in a transit. The abbreviation 'FFT' will be adopted for this direct fast Fourier transform method.

The last method requires the opposite: here the phase of the integrand needs to be rapidly varying. The first two methods are best suited to describe the Landau or TTMP interaction (in which case no cyclotron frequency appears in the phase of the integrand), while the third is best suited to describe the cyclotron interaction: since the cyclotron frequency is typically a factor of 1000 larger than the bounce frequency, the poloidal inhomogeneity of the cyclotron frequency results in rapid phase variations during a bounce. When referring to the adopted asymptotic stationary-phase technique, the label 'SP' will be used.

Louis (1995) demonstrated that the FFT and asymptotic methods are complementary: one is computationally fast when the other is slow, and vice versa.

4.1. A first crude model for cyclotron interaction

Before trying to derive expressions for $\mathscr{B}_N$ that hold for various different heating scenarios and orbits, it is useful to explore the simplest possible case, i.e. the case that bears the closest resemblance to familiar uniform or quasi-uniform plasma expressions. Ideally, this would amount to expressions in which the uniform plasma expressions can immediately be recognized. In view of the great many steps, only a sketch of the philosophy will be given here. For details, the reader is referred to the papers of Van Eester and Lamalle (and the references therein) in the reference list. One ingredient that one desires to appear is the resonant denominator $k_\parallel v_\parallel + N\Omega - \omega$. It is known that if the phase of the RF-induced energy change varies rapidly as a function of the bounce angle, the stationary-phase method can be used

https://doi.org/10.1017/S0022377801001246 Published online by Cambridge University Press

to evaluate the bounce integral in the definition of $\dot{\varepsilon}_{\mathbf{m}}$. As the stationary-phase condition is $k_{\|}v_{\|} + N\boldsymbol{\Omega} = \mathbf{m}\cdot\boldsymbol{\omega}$ (see e.g. equation (21) in Van Eester 1998) and the resonance condition $\mathbf{m}\cdot\boldsymbol{\omega} = \omega$, the desired resonance condition appears. Orbits on which there is appreciable variation of $\boldsymbol{\Omega}$ are thus likely candidates to serve our present purpose. In the present section, we implicitly assume that $N \neq 0$, that the considered magnetic surface is not too close to the magnetic axis and that the orbit is not deeply trapped.

For cyclotron interaction, away from the magnetic axis and excluding deeply trapped orbits, the stationary-phase method is well suited to evaluate the bounce integral (see e.g. Van Eester (1995, 1998) for the genera1 procedure, and see further for more details on practical formulae). In that case, the bounce spectrum consists of many modes (since the stationary-phase condition is $m_b\omega_b + m_d\omega_d + m_g\omega_g = k_{\|}v_{\|} + N\boldsymbol{\Omega}$, the bounce spectrum has of order $\boldsymbol{\Omega}/\omega_b$ modes when $N \neq 0$) and thus the stationary-phase points are densely packed: the many bounce modes correspond to as many stationary-phase points. Nearby bounce modes are thus expected to have nearby stationary-phase points. In case the simplest decorrelation model is adopted ($\omega \rightarrow \omega + i\nu$) and decorrelation is sufficiently rapid (ν sufficiently large; see also Sec. 4.2), many of these bounce modes contribute to absorption, and therefore one can replace the sum on the bounce modes by a bounce integral. The function $\mathscr{B}_N$ in (16) is the square of a quantity involving the total electric field. It can therefore be written as a double sum on the poloidal mode m_1 and m_2. Making a Taylor expansion of the phase factor in the stationary-phase expression around the average poloidal mode $\frac{1}{2}(m_1 + m_2)$, the combined phase factor takes the simple form $(m_1 - m_2)\theta$ and so the factor $\mathscr{B}_N$, can be written as follows (Lamalle 1997; Van Eester 1999):

$$\begin{aligned}\mathscr{B}_N &= \frac{1}{2}\mathrm{Re}\left\{\left(\frac{q_s}{m_s}\right)^2 \sum_n \sum_{m_1} \sum_{m_2} \frac{1}{2\pi}\right.\\ &\left.\times \int_0^{2\pi} d\Phi_b \, \frac{\mathscr{L}_{m_1}(\mathbf{E}_{m_1}(\rho))\mathscr{L}^*_{m_2}(\mathbf{E}_{m_2}(\rho))\,\exp[i(m_1 - m_2)\theta]}{i(k_{\|}v_{\|} + N\boldsymbol{\Omega} - \omega)}\right\}\\ &= \left(\frac{q_s}{2m_s}\right)^2 \sum_n \sum_{m_1} \sum_{m_2} \sum_{\mathrm{res}} \frac{\mathrm{Re}\{\mathscr{L}_{m_1}(\mathbf{E}_{m_1}(\rho))\mathscr{L}^*_{m_2}(\mathbf{E}_{m_2}(\rho))\,\exp[i(m_1 - m_2)\theta]\}}{\omega_b \left|d^2\Xi/d\Phi_b^2\right|}.\end{aligned} \tag{17}$$

The parallel wavenumber in the above is that associated with the average poloidal mode number. The resonant positions thus depend on both m_1 and m_2, The operator $\mathscr{L}$ in the above is that due to Kennel and Engelmann (1966):

$$\mathscr{L}\mathbf{E} = \tfrac{1}{2}v_{\perp}(J_{N+1}e^{i(N+1)\Psi}E_- + J_{N-1}e^{i(N-1)\Psi}E_+) + v_{\|}J_N e^{iN\Psi}E_{\|}, \tag{18a}$$

$$J_L e^{iL\Psi} = \left(-i\frac{v_{\perp}}{2\Omega}\nabla_-\right)^L \sum_{j=0}^{\infty}\left(\frac{v_{\perp}}{2\Omega}\right)^{2j}\frac{\Delta_{\perp}^j}{j!(L+j)!}, \tag{18b}$$

$$J_{-L}e^{-iL\Psi} = \left(+i\frac{v_{\perp}}{2\Omega}\nabla_+\right)^L \sum_{j=0}^{\infty}\left(\frac{v_{\perp}}{2\Omega}\right)^{2j}\frac{\Delta_{\perp}^j}{j!(L+j)!}, \tag{18c}$$

$$\nabla_{\pm} = (\mathbf{e}_{\perp 1} \mp i\mathbf{e}_{\perp 2})\cdot\boldsymbol{\nabla}. \tag{18d}$$

https://doi.org/10.1017/S0022377801001246 Published online by Cambridge University Press

Here Ψ is the angle between $\mathbf{k}_\perp$ and $\mathbf{e}_{\perp 1}$, $\Delta_\perp$ is the perpendicular Laplace operator, L is positive or zero, $\mathbf{e}_{\perp 1} = \mathbf{e}_\rho$ and $\mathbf{e}_{\perp 2} = \mathbf{e}_\parallel \times \mathbf{e}_\rho$. The expression (17) suggests that the way to generalize uniform plasma expressions is straightforward: after substantial algebra, one finds that it suffices to account for the full poloidal spectrum of the field and to perform a bounce average. Both are 'intuitive' generalizations that one expects when going to a poloidally non-uniform plasma. The appealing simplicity hides a weakness, however: whereas the genera1 expression (8) guarantees a strictly positive power absorption for a Maxwellian plasma (which is what one expects), the above expression does not: considering two differing poloidal modes and the four corresponding contributions ($[m_1, m_1], [m_1, m_2], [m_2, m_1]$ and $[m_2, m_2]$) to the above sum, one finds two strictly positive and two complex-conjugate contributions to be evaluated at three different SP points, namely the SP points corresponding to $m = m_1$, $m = m_2$ and $m = \frac{1}{2}(m_1 + m_2)$ respectively. The former do not pose a problem for the positivity of the result, but the sum of the latter two does not have a definite sign. A numerical example for a monomodal field (in which no problem occurs) as well as an example for a multimodal field (in which positivity is not guaranteed) is shown in Fig. 1. Shown is the vv coefficient $Q_{vv} = \mathscr{B}_N/v^2$ of the diffusion operator $Q = (1/J)(\partial/\partial v)JQ_{vv}\partial/\partial v + \ldots$ (see (7)) for a costreaming ^{3}He population in TEXTOR. In this paper, the labels 'co' and 'counter' are with reference to the static magnetic field direction, not the plasma current. The major radius $R_0 = 1.75\,\mathrm{m}$, the magnetic surface is circular and has minor radius $r = 0.15\,\mathrm{m}$, the toroidal mode number $n = -13$, the radial wave vector component is $40\,\mathrm{m}^{-1}$, the frequency $f = 38\,\mathrm{MHz}$, the central toroidal magnetic field $B_0 = 1.8\,\mathrm{T}$, and the (for circular surfaces constant) angle between the parallel and the toroidal direction is $\alpha = 0.15$. In the region in c.o.m. space that corresponds to the tangent resonance region on the magnetic surface, the predicted Q_{vv} is unphysical (negative!) and rapidly varying, while it is well behaved in velocity regions corresponding to resonances away from the turning points.

The expression (17) for the active dielectric response of a toroidal plasma is not the only one proposed in the literature. In attempts to try to guarantee a positive-definite power absorption for a Maxwellian tokamak plasma, various expressions for the dielectric response have been obtained (see e.g. Jaeger et al. 1998; Brambilla 1999). When the wave equation is written using a weak Galerkin form, the positive-definiteness requires the symmetry of the operator acting on the test function (which becomes the electric field if the power conservation law is looked at) and acting on the wave field, and requires the resonant denominator to be independent of a specific poloidal mode. Although the Kennel–Engelman operator can easily be made symmetric (see Colestock and Kashuba (1983) for dominant terms and Van Eester and Koch (1988) for all up to second-order finite-Larmor-radius terms), the resonant denominator (arising from the time-history integral in the expression for the perturbed distribution function) contains the poloidal mode number of the electric field via the parallel wavenumber in the Doppler-shift factor $k_\parallel v_\parallel$. Kaufman's expressions *do* guarantee this symmetry and independence, and so it seems logical to return to his philosophy to derive the wave and associated Fokker–Planck equations. The expression (17) starts from Kaufman's expressions, but relies on a truncated Taylor series expansion of the phase factors corresponding to the two poloidal modes m_1 and m_2 of the field and test function, and yields, upon dropping higher-order corrections, a symmetrized expression for the resonant denominator. Because the resonant denominator still explicitly contains poloidal mode numbers,

https://doi.org/10.1017/S0022377801001246 Published online by Cambridge University Press

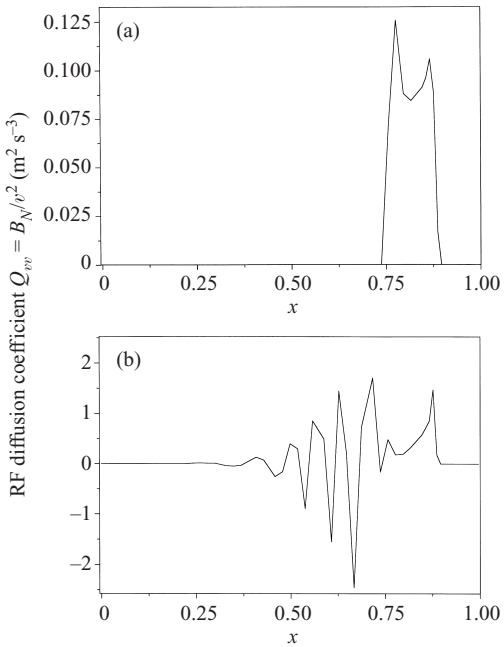

Figure 1. The RF diffusion coefficient Q_{vv} for a co-streaming ^{3}He particle population heated at $\omega = 2\Omega_{^3\mathrm{He}}$ in the TEXTOR tokamak. Simple analytical wave field amplitudes are used: (a) result for the monomodal field with poloidal mode number $m = -6$ and (b) result for a multimodal field with 13 poloidal mode numbers ranging form -6 to $+6$. The result is given for $v = 3 \times 10^6\,\mathrm{m\,s^{-1}}$.

positivity, however, still cannot be guaranteed, unless the Doppler shift is omitted altogether. This was done in Belikov and Kolesnichenko (1982). In that particular case, the numerator can be rewritten as the sum over the poloidal modes of the absolute value of the Fourier mode squared. Since this is not justified in general, because the Dopple shift is small but essential, the basic problem remains: although it seems a logical generalization of the uniform-plasma expression, the exponential factor $\exp[i(m_1 - m_2)\theta]$ prevents the power absorption from being positive-definite. *All* expressions that contain this factor but have poloidal mode dependence in the resonant denominator face this limitation. In the expressions of Kaufman, the resonant denominator depends on the bounce mode, not the poloidal mode, and thus the summation in the numerator can justifiably be performed.

4.2. Decorrelation: a note on 'collisionless' damping

The computationally most appealing evaluation relies on asymptotic techniques. Combining the stationary-phase condition $k_\parallel v_\parallel + N\boldsymbol{\Omega} = \mathbf{m} \cdot \boldsymbol{\omega}$ and the resonance condition $\mathbf{m} \cdot \boldsymbol{\omega} = \omega$ yields the resonant bounce mode number $m_{b_{\mathrm{res}}}$. Note that causality commonly yields a real rather than an integer resonant mode number. Strictly speaking, the absorption is thus only non-zero on a discrete number of surfaces on which this real number is an integer! This at first sight unfamiliar result unveils inaccurate nomenclature: the term 'collisionless' damping plasma is unfortunate for a tokamak plasma, since the absorption referred to depends critically on collisions or, more generally, some other decorrelation mechanism. This is most evident on looking at the resonant denominator and how it is related

https://doi.org/10.1017/S0022377801001246 Published online by Cambridge University Press

to damping. We start from the (quasi-)uniform plasma case for which the total absorbed power $P_{\rm abs}$ is of the form

$$P_{\rm abs} = \frac{1}{2}{\rm Re}\left\{\int d\mathbf{x}\,\mathbf{E}^*\cdot\mathbf{J}\right\} = \frac{1}{2}{\rm Re}\left\{\ldots\int d\mathbf{v}\,d\mathbf{x}\frac{\ldots}{i(k_\parallel v_\parallel + N\boldsymbol{\Omega}-\omega)}\right\}$$

Since collisionality can be accounted for in the dielectric response by identifying a finite ν with the collision frequency ν_c, since $\nu_c \ll \omega$ and since it makes no difference in practice if ν is taken very small or infinitesimal ($\nu \to 0^+$), the term 'collisionless' damping is justified in the (quasi-)uniform case. Absorption takes place when $k_\parallel v_\parallel + n\boldsymbol{\Omega} - \omega = 0$. In a tokamak, the absorbed power $P_{\rm abs}$ in a volume delimited by two magnetic surfaces is given by

$$P_{\rm abs} = \frac{1}{2}{\rm Re}\left\{\int d\mathbf{x}\,\mathbf{E}^*\cdot\mathbf{J}\right\} = \frac{1}{2}{\rm Re}\left\{(\ldots)\sum_{\mathbf{m}}\int d\boldsymbol{\Lambda}\,\frac{(\ldots)}{i(\mathbf{m}\cdot\boldsymbol{\omega}-\omega)}\right\},$$

which is closely related to the uniform-plasma expression: for the particular case of well-passing particles in a tokamak with circular cross-section, the relations $\omega_b \approx v_\parallel \sin\alpha/r$ and $\omega_d \approx v_\parallel\cos\alpha/R$ hold, and the bounce and poloidal mode numbers coincide, so the uniform resonance condition is recaptured, except that the orbit is helicoidal and not straight. The above expression is thus closely related to that of the uniform case for that particular situation.

There is, however, one important difference between the two cases: in the first, the total absorption is an *integral* over the continuous wave spectrum, while, owing to the periodicity of the geometry, it is a discrete *sum* on the mode spectrum in the tokamak. It is instructive to study the behaviour of the function

$${\rm Re}\left\{\frac{1}{i[\mathbf{m}\cdot\boldsymbol{\omega}-(\omega+i\nu)]}\right\} = \frac{1}{\omega_b}\frac{\nu/\omega_b}{(m_b - m_{b_{\rm res}})^2 + (\nu/\omega_b)^2},$$

with

$$m_{b_{\rm res}} = \frac{\omega - m_d\omega_d - m_g\omega_g}{\omega_b}, \tag{19}$$

as a function of the bounce mode number and the parameter $\nu \ll \omega$. In the case where m_b is a continuous variable varying from $-\infty$ to $+\infty$, this function is peaked around the resonant bounce mode and the integral of the function is always π/ω_b, independent of the exact value of ν. The width of the peak depends on the magnitude of ν with respect to ω_b. If ν/ω_b is large, then this function is non-negligible in a very wide interval of m_b values. If it is small, then the function is very strongly peaked around the resonant mode. In the limit $\nu \to 0^+$, a delta function appears. In the case where m_b is a discrete integer rather than a continuous real variable, the local value of the function in (19) is the same as before, but, depending on the magnitude of ν/ω_b, the discrete sum and the continuous integral may be very different: for small ν/ω_b, the function is poorly sampled and the sum is much smaller than the integral, the extreme situation being that where the resonant bounce mode lies between two integer bounce modes, and the width of the curve is much smaller than 1 (the distance between two integer m_b values). In that case, the integral is still π/ω_b while the sum is zero!

The consequence of the $k_\parallel$ quantization is that the condition $\nu \ll \omega$ no longer uniquely defines the 'collisionless' regime. Since the bounce frequency is small with respect to ω as well, three different regimes now occur. When the decorrelation

https://doi.org/10.1017/S0022377801001246 Published online by Cambridge University Press

frequency is large with respect to the bounce frequency, the sum over the bounce spectrum yields essentially the same result as the bounce integral, as just explained. Note, however, that ν is necessarily non-zero (i.e. the regime is essentially *collisional* when thinking of ν as a collision frequency), since it is *large* compared with ω_b. When, on the contrary, the bounce frequency is large compared with ν, the same reasoning yields a regime much more entitled to the label 'collisionless', but only in the exceptional case when the above-defined $m_{b_{\rm res}}$ is an integer is the absorption non-zero. The smaller is ν, the smaller is the probability to have finite absorption for a given set of constants of motion. The bounce integral and the sum over the bounce spectrum now yield two totally different results: the integral still picks up the delta-function contribution at the local resonance and predicts the same damping as in the previous case, while the bounce sum usually picks up negligible contributions and predicts poor or no damping. Although truly entitled to the name 'collisionless' damping, this regime (known as the superadiabatic regime – Faulconer and Liboff 1972) is not what is commonly understood when referring to collisionless damping. Rather than being localized at the poloidal position satisfying the resonance condition $k_\parallel v_\parallel + N\Omega - \omega = 0$, this damping occurs globally on a finite set of magnetic surfaces. A third regime occurs when ω_b and ν are comparable. Constructive or destructive interference of various encounters of a particle with the same resonance is then important. This is the only regime where the details of the decorrelation model actually matter (for an example, see Van Eester et al. 1996).

Two of the above three regimes do not exist in the uniform-plasma case. The fundamental difference is not caused by the *toroidicity* but by the poloidal field needed for the plasma's stability: the poloidally *closed* orbits give rise to a supplementary class of particles (trapped versus passing particles) and to a different absorption phenomenon (global versus local absorption). This is how 'quasi-uniform' needs to be interpreted: as long as relevant quantities only exhibit modest variations and as long as the orbit is open, no conceptually new physics is added to the RF-heating model. It does, however, not yield new insights.

The decorrelation frequency in (19) is not directly to be interpreted as a collision frequency. Adopting a simplified collision operator, Kasilov pointed out that the decorrelation frequency associated with the collisions is significantly larger than the collision frequency itself. Consequently, collisions are expected to yield a decorrelation time that is short on the transit time scale but long on the cyclotron time scale (Kasilov et al. 1990). Other decorrelation mechanisms not involving collisions (e.g. Hamiltonian stochastization of the electric field itself) may equally suffice to decorrelate a particle on its orbit. It is sufficient that in the typically $O(1000)$ gyrorevolutions that a particle makes in a bounce, the parallel velocity is deflected by 1/1000 to completely decorrelate the particle on a bounce. If decorrelation is sufficiently fast, the resonance function is non-zero for a large number of bounce modes (corresponding to many densely spaced resonant positions contributing to the total wave absorption), and thus the sum over the resonant modes is almost equivalent to an integral over the resonant positions. From that point of view, it is plausible to let the unique resonant bounce mode be a real number to guarantee finite damping on every magnetic surface. Mathematically, this is not a very satisfying procedure: periodic functions are fully described by a set of basis functions $\exp(im_b\Phi_b)$ with integer m_b. A better and mathematically rigorous description is to add the decorrelation physics by adopting a more general decorrelation function

(see e.g. Louis 1995; Van Eester et al. 1996). For the physical regime of interest, this yields a sum over many bounce-mode contributions, and thus leads to a significantly longer computation time, but does not give new insights.

4.3. Back to basics: a better model for cyclotron interaction

Crudely speaking, positivity is guaranteed when the stationary-phase points corresponding to m_1 and m_2, lie very close to each other (in which case the numerator of the above sum combines approximately to the absolute value of the sum on the poloidal modes). This is often guaranteed, but two important exceptions occur:

(i) When the mode numbers themselves are very different, the corresponding stationary-phase points differ significantly as well.

(ii) Even when the poloidal mode numbers do not differ much, the stationary-phase points are widely spaced near turning points.

A numerical demonstration of the spacing for both cases can be found in Van Eester (1997). Remembering that the bounce and cyclotron frequency differ from one another by typically a factor of 10^3, and realizing that in the case of $N \neq 0$, the phase function contains the rapidly varying cyclotron gyration term, one sees that a small but perfectly acceptable relative error of order 10^{-3} on the cyclotron term in the Taylor series corresponds to an error/indetermination of a full poloidal bounce! The applicability of the Taylor series expansion for more or less distant stationary-phase points is therefore arguable. Near the turning points in the equatorial plane, the wide spacing occurs even if the poloidal mode numbers are not very different. Both the arguments just above and the discussion of 'collisionless' damping in a tokamak indicate that the replacement of the bounce sum by a bounce integral is not trivially justifiable there. The wide spacing between stationary-phase points corresponding to different bounce modes and/or poloidal modes is not an argument for not using asymptotic techniques to evaluate the Fourier amplitudes, however. It just prevents one from further simplifying the product of the expressions for two modes by relating not so nearby SP points via approximate phase conditions. Adopting a Taylor series expansion truncated at second-order terms for the phase, an individual Fourier component can be approximated by

$$
\begin{aligned}
(\mathbf{E}\cdot\mathbf{v})_{\mathbf{m}} &= \frac{1}{2\pi}\int_0^{2\pi} d\Phi_b\, \mathscr{L}e^{i\Theta} = \sum_{spp} \frac{\mathscr{L}e^{i[\Theta+\mathrm{sign}(\Theta'')\,\pi/4]}}{(2\pi)^{1/2}|\Theta''|^{1/2}} \\
&= \frac{\mathscr{L}e^{i[\Theta+\mathrm{sign}(\Theta'')\,\pi/4]}}{(2\pi)^{1/2}|\Theta''|^{1/2}} + \frac{\mathscr{L}e^{-i[\Theta+\mathrm{sign}(\Theta'')\,\pi/4]}}{(2\pi)^{1/2}|\Theta''|^{1/2}} \\
&= \left(\frac{2}{\pi}\right)^{1/2} \left.\frac{\mathscr{L}\ \cos[\Theta+\mathrm{sign}(\Theta'')\,\pi/4]}{|\Theta''|^{1/2}}\right|_{\mathrm{up}},
\end{aligned}
\tag{20}
$$

in which $\mathscr{L}$ is the previously mentioned Kennel–Engelman operator and

$$
\Theta(\Phi_b) = \Xi(\Phi_b) - \mathbf{m}\cdot\mathbf{\Phi} = \Xi(\Phi_b) - \frac{m_b\omega_b + n\omega_d - N\omega_g}{\omega_b}\Phi_b. \tag{21}
$$

The poloidal mode number m, the toroidal mode number $n = m_d$, the gyro mode number $N = -m_g$ and the bounce mode number m_b are implicit in (21). In the sum on the first line of (20) the functions are evaluated at the stationary-phase

https://doi.org/10.1017/S0022377801001246 Published online by Cambridge University Press

points, satisfying

$$\Theta'(\Phi_b) = 0 \quad \text{or} \quad \dot{\Theta}(\Phi_b) = 0, \quad \text{i.e.} \quad k_\parallel v_\parallel + N\Omega = \mathbf{m}\cdot\boldsymbol{\omega} \tag{22}$$

($' = \partial/\partial\Phi_b$ and $\dot{} = d/dt$). In the second line of (19), everything has been expressed as a function of the stationary-phase point above the midplane and use has been made of the fact that the chosen equilibrium is up–down-symmetric. As can be seen in (18) and (21), and using (13), $\mathscr{L}$ has the same value for the two stationary-phase points, but Θ changes sign: $\mathscr{L}$ involves the electric field amplitude (and its radial and poloidal derivatives), the cyclotron frequeny, and the parallel and the perpendicular velocity, which are symmetric about the midplane for an up–down-symmetric equilibrium, while Θ involves Φ_b and $\sin(l\ \Phi_b)$ terms. The two stationary-phase point contributions can then be grouped in a single one. In case of an up–down-asymmetric equilibrium, the cos factor in (20) is wrong, although the expression with the sum over the stationary-phase points is still correct. The resonant denominator in the expression for the dielectric response now reduces to its familiar form $k_\parallel v_\parallel + N\Omega - \omega$. At no point, however, do we associate a single stationary-phase point of a particular poloidal mode with this resonant denominator. Via the resonance condition, the resonant bounce mode $m_{b_{\text{res}}}$, and thus the resonant denominator is a fixed quantity for fixed v and x. For this fixed resonant denominator, different stationary-phase points are obtained for different poloidal mode numbers. The Fourier amplitude of the total RF-induced energy change (summed over the poloidal spectrum) is the sum of the obtained stationary-phase point contributions for the various poloidal mode numbers. The square of the absolute value of this total Fourier amplitude appears in the RF diffusion coefficient and the absorbed power density.

4.4. Tangent resonance: Is more detailed necessarily better?

When the second derivative of the phase goes to zero (turning point), the simple stationary-phase evaluation becomes invalid and a higher-order expansion is needed. The expression for the bounce-mode amplitude for a cubic approximation of the phase is

$$\begin{aligned}(\mathbf{E}\cdot\mathbf{v})_{\mathbf{m}} &= \frac{1}{2\pi}\int_0^{2\pi} d\Phi_b\ \mathscr{L}e^{i\Theta} \approx \frac{\mathscr{L}\ e^{i\Theta_{tp}}}{\left|\Theta'''_{tp}\right|^{1/3}}\mathrm{Ai}\left(-\frac{|\Theta'_{tp}|}{\left|\frac{1}{2}\Theta'''_{tp}\right|^{1/3}}\right)\\ &\approx \frac{\mathscr{L}_{tp}e^{i(\Theta_{spp}+\Theta'^3_{spp}/3\Theta'''^2_{spp})}}{\left|\frac{1}{2}\Theta'''_{spp}\right|^{1/3}}\mathrm{Ai}\left(-\frac{\left|\Theta''^2_{spp}\right|}{\left|2^{2/3}\Theta'''^{4/3}_{spp}\right|}\right),\end{aligned} \tag{23}$$

which can be expressed in terms of the stationary-phase point or of the nearby turning point. Using the cubic approximation of the phase Θ, one can find an expression relating the derivatives $\Theta^n (n = 0,\ldots,3)$ at the stationary-phase point (spp) and those at the turning point (tp). One finds

$$\left.\begin{aligned}
&\Theta_{tp} = \Theta_{spp} - \tfrac{1}{3}\Theta'''_{spp}\Delta^3, && \Theta_{spp} = \Theta_{tp} + \tfrac{1}{3}\Theta'''_{tp}\Delta^3,\\
&\Theta'_{tp} = -\tfrac{1}{2}\Theta'''_{spp}\Delta^2, && \Theta'_{spp} = 0,\\
&\Theta''_{tp} = 0, && \Theta''_{spp} = -\Theta'''_{tp}\Delta,\\
&\Theta'''_{tp} = \Theta'''_{spp}, && \Theta'''_{spp} = \Theta'''_{tp},\\
&\Delta = \Phi_{b_{tp}} - \Phi_{b_{spp}} = -\frac{\Theta''_{spp}}{\Theta'''_{spp}}, && \Delta = \pm\left(\frac{-2\Theta'_{tp}}{\Theta'''_{tp}}\right)^{1/2}.
\end{aligned}\right\} \tag{24}$$

https://doi.org/10.1017/S0022377801001246 Published online by Cambridge University Press

The subscripts of the various functions refer to the position at which the functions are evaluated. For real stationary-phase points, the cubic approximation prescribes that the first and third derivatives of the turning-point phase are of opposite sign, and that the stationary-phase points lie symmetrically about the turning point, at which the second derivative changes sign.

It is tempting to always use this higher-order formula. Note, however, that the cubic expansion (with coefficients evaluated at the true stationary-phase point) always predicts a nearby turning point and symmetric about this approximate 'cubic' turning point, a second stationary-phase point. Neither the turning point nor the second stationary-phase point have any physical significance *except* when the 'cubic' turning point coincides with the actual turning point. The above expression, which *always* contains the contribution of two correlated stationary-phase points, thus cannot trivially be used as a better approximation. This becomes more clear when the asymptotic expression (well-separated stationary-phase points) is considered:

$$(\mathbf{E}\cdot\mathbf{v})_{\mathbf{m}} \approx \frac{\mathscr{L}_{tp}e^{i\Theta_{tp}}}{|2\Theta'_{tp}\Theta'''_{tp}|^{1/4}}\left(\frac{2}{\pi}\right)^{1/2}\cos\left(\frac{2^{3/2}|\Theta'_{tp}|^{3/2}}{3|\Theta'''_{tp}|^{1/2}}-\frac{\pi}{4}\right). \tag{25}$$

Writing the cosine as the sum of two exponential factors and using (24), one recognizes the two contributions of the earlier found simple form given in (20). This demonstrates that the simple and higher-order expressions are in agreement when both are valid, as one would expect. One of the terms in (25) corresponds to one of the *physical* contributions appearing in (20) (in the phase factor of the exponential, the terms involving the derivatives of the phase at the stationary-phase point cancel for this stationary-phase point). The other stationary-phase point (and the associated turning point halfway between the two stationary-phase points of the cubic phase) is, however, an *artefact* of the cubic truncation of the phase. Adopting (23) to evaluate the RF-induced energy change thus yields *erroneous* results, each stationary-phase point contribution in (23) containing a physical and an unphysical part, the latter giving rise to artificial interference.

In the light of the wider spacing of the stationary-phase points near a turning point, one may wonder if the more accurate expression is of much use. If the 'cubic' turning point coincides with the actual turning point (which means that the truncated Taylor series with coefficients evaluated at the stationary phase point is still valid at the true turning point, notwithstanding the relatively large phase difference between two points), the higher-order expression must be used instead of the diverging sum of the two saddle-point contributions of the simple asymptotic expression. If the 'cubic' turning point does not coincide with the actual one (i.e. the – relatively small – errors in the phase cause non-negligible errors in the predicted positions for the nearby turning point and the second stationary-phase point), the higher-order expression is strictly invalid, but is expected to be more physically relevant than the predictions from the simple expression, since the latter diverges unphysically. Because of this divergence, the prediction using the higher-order expression is therefore preferred for stationary-phase points very close to the true turning point, but it must be realized that the interference pattern it shows is not necessarily physically correct.

4.5. Čerenkov interaction and/or orbits with limited extent

When the phase does not vary rapidly, the stationary-phase point evaluation technique no longer predicts the Fourier amplitude correctly. In this case, a fast Fourier

https://doi.org/10.1017/S0022377801001246 Published online by Cambridge University Press

transformation or a brute numerical integration of the integral yields a better approximation. Another possibility is to benefit from the fact that a small number of Fourier modes contribute significantly to the integral, allowing one to perform the integral in (20) semi-analytically. The first step is to find the Fourier spectrum of the slowly varying factor $\mathscr{L}$ in the integrand. This may be done using the FFT on a limited set of Φ_b grid points using (13). The next step is to write the exponential in the integrand as a product of sums of Bessel functions, relying on (Abramowitz Stegun 1964)

$$e^{i\xi \sin\gamma} = \sum_{k=-\infty}^{+\infty} J_k(\xi) e^{ik\gamma}.$$

Rather than having to consider an infinite series of products, one may truncate the product at a term for which all but the zeroth-order Bessel functions are negligible (the amplitude of the Fourier series of the phase is smaller than any desired accuracy beyond a certain index; for an example, see Van Eester (1998)). The different sums in the product can be truncated as well: for a given argument ξ, the Bessel function becomes small if its index exceeds $0.5\xi e$ (see Abramowitz and Stegun 1964). One gets

$$\begin{aligned}
\dot{\varepsilon}_{\mathbf{m}} &= \frac{1}{2\pi}\int_0^{2\pi} d\Phi_b \mathscr{L} e^{i\Theta} \approx \sum_{j=-j_{\max}}^{j_{\max}} \mathscr{L}_j \frac{1}{2\pi}\int_0^{2\pi} d\Phi_b\, e^{ij\Phi_b} \exp\left(i\sum_{k=-k_{\max}}^{k_{\max}} \xi_k \sin\Phi_b\right) \\
&\approx \sum_{j=-j_{\max}}^{j_{\max}} \mathscr{L}_j \frac{1}{2\pi}\int_0^{2\pi} d\Phi_b\, e^{i(\xi_0+j)\Phi_b} \\
&\quad \times \left[\sum_{k'=-k'_{\max}}^{k'_{\max}} J_{k'}(\xi_{-k_{\max}}) e^{ik'(-k_{\max})\Phi_b}\right] \cdots \left[\sum_{k''=-k''_{\max}}^{k''_{\max}} J_{k''}(\xi_{k_{\max}}) e^{ik''(+k_{\max})\Phi_b}\right] \\
&\approx \sum_{j=-j_{\max}}^{j_{\max}} \mathscr{L}_j \sum_{k'=-k'_{\max}}^{k'_{\max}} J_{k'}(\xi_{-k_{\max}}) \cdots \sum_{k''=-k''_{\max}}^{k''_{\max}} J_{k''}(\xi_{k_{\max}}) \frac{1}{2\pi} \\
&\quad \times \int_0^{2\pi} d\Phi_b\, e^{i(\xi_0+j-k'k_{\max}+\cdots+k''k_{\max})\Phi_b},
\end{aligned} \tag{26}$$

in which j is the Fourier-component index of $\mathscr{L}$ ($-j_{\max} \leqslant j \leqslant j_{\max}$), k is the Fourier-component index of the phase Ξ (see (15); $-k_{\max} \leqslant k \leqslant k_{\max}$), k' is the index of the series corresponding to the first ξ ($\xi_{k_{\max}}$; $-k'_{\max} \leqslant k' \leqslant k'_{\max}$,) in the Fourier series of Ξ, k'' is the index of the last one, and the '...' represent the various of contributions of the intermediate ks. Owing to the large number of relevant Fourier modes of the phase (and, to a lesser extent, of $\mathscr{L}$), and to the fact that each of the Fourier components of the phase gives rise to a sum of terms, the final expression contains many terms unless $N = 0$. The last step of the computation is straightforward: grouping the various exponential factors, the integral can be evaluated analytically. The result is only non-zero when the factor $j + \xi_0 - k'k_{\max} + \ldots + k''k_{\max}$ is zero. Although the above formula is in principle valid for slowly as well as rapidly varying phases, it is evident that the large number of terms to be kept and the associated

https://doi.org/10.1017/S0022377801001246 Published online by Cambridge University Press

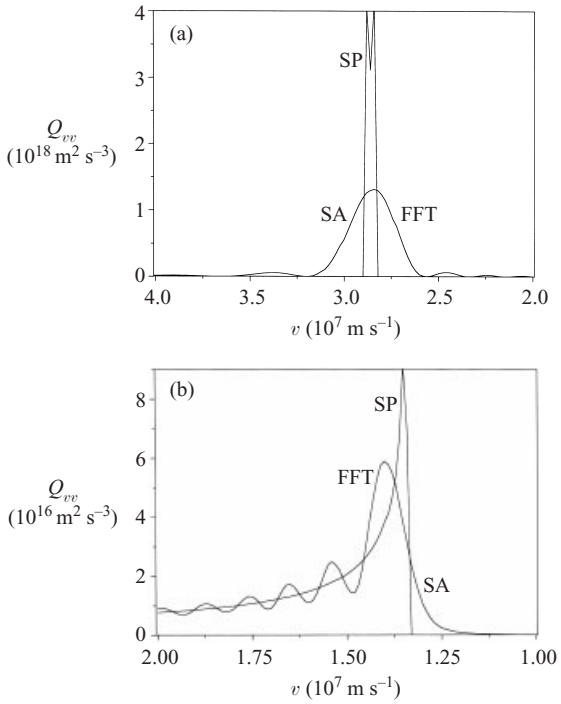

Figure 2. The RF diffusion coefficient Q_{vv} for an electron population heated by Landau or TTMP damping in the JET tokamak. Simple analytical wave field amplitudes are used and uncorrelated resonances are assumed. The toroidal mode number is (a) $n = +18$ or (b) $n = 180$; the plots are for (a) $x = 0.45$ and (b) x=0.95. The labels SP, SA and FFT indicate the method used to evaluate the coefficient (stationary-phase, semi-analytical and fast Fourier transform technique, respectively).

'bookkeeping' to be done make it numerically unattractive when many terms have to be kept in the Fourier series.

4.6. Numerical examples: the structure of the RF diffusion coefficients

4.6.1. Performance of the various methods. The asymptotic and FFT methods are complementary: when one cannot be used, the other most easily yields an accurate result. A detailed discussion can be found in Louis (1995), in which not only the active (as is done here) but also the reactive contributions to the dielectric response were computed. Figure 2 shows the diffusion coefficient for an electron population in JET heated by Čerenkov interaction ($N = 0$). The major radius $R = 3.1$ m, the minor radius is 1.25 m, the magnetic surface is a Shafranov-shifted D with equatorial half-width $\rho = 0.2$ m, the elongation is 1.6, Shafranov shift of the magnetic axis is 0.3 m and the triangularity is 0.3, the poloidal mode number $m = 6$, the radial wave vector component $k_\rho = -30\,\mathrm{m}^{-1}$, the frequency $f = 26$ MHz, the central toroidal magnetic field $B_0 = 3.1$ T, and the angle between the parallel and the toroidal direction is $\alpha = 0.15$ at the outboard side of the equatorial plane. Figure 2(a) is the result when the toroidal mode number $n = 18$. The (physically correct) predictions of the SA formula (26) and the FFT coincide, while those of the (failing) stationary-phase method predicts a narrower and higher peak. Only the first three terms in the Fourier spectrum of the phase are retained in the SA model,

https://doi.org/10.1017/S0022377801001246 Published online by Cambridge University Press

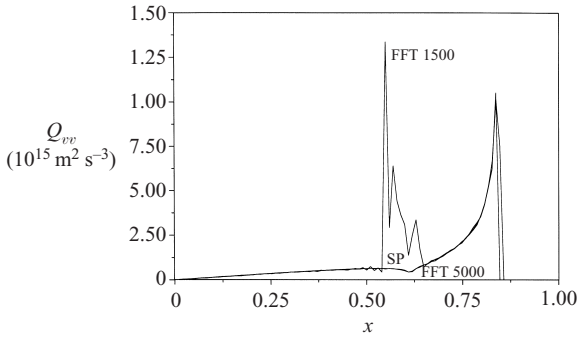

Figure 3. The RF diffusion coefficient Q_{vv} for a co-streaming H population heated on axis at its fundamental cyclotron frequency in the JET tokamak. Simple analytical wave field amplitudes are used and uncorrelated resonances are assumed. The velocity $v = 10^6\,\mathrm{m\,s^{-1}}$.

and the maximal number of Bessel functions considered is limited. When $n = 180$, one sees that the prediction of the asymptotic method is already in better agreement with the (correct) FFT prediction, as one expects for a more rapidly varying phase. For the case of cyclotron heating, the bounce spectrum of the RF induced energy change containing a few thousand modes, and an oscillation being reasonably well captured by $O(20)$ points per period, one needs $O(10^5)$ points to capture the most rapid oscillations when using the FFT method. Happily a somewhat smaller number suffices to get a reasonably good approximation. This is illustrated in Fig. 3, showing both the FFT and SP point prediction for a cyclotron heating case. The major radius $R_0 = 3.12\,\mathrm{m}$, the magnetic surface has a D-shaped cross-section with half-width $\rho = 0.8\,\mathrm{m}$, an elongation of 1.6, and a triangularity of 0.3. The Shafranov shift of the magnetic axis is 0.3 m. The toroidal mode number $n = +20$, the poloidal mode number $m = 5$ and the radial wave vector component $k_\rho = -30\,\mathrm{m^{-1}}$. The frequency $f = 47.13\,\mathrm{MHz}$, the central toroidal magnetic field $B_0 = 3.4\,\mathrm{T}$, and the angle between the parallel and the toroidal direction is taken as $\alpha = 0.15$ at the outboard side of the equatorial plane. For the parameters taken, both methods roughly agree when 5000 Φ_b points are used to evaluate the bounce integral. When only 1500 points are used, the FFT integration fails to predict the correct coefficient near the trapped/passing boundary. In either case, the FFT procedure requires much more CPU time to estimate the bounce integral than the asymptotic technique does. Louis showed that accounting for a finite decorrelation time has an advantage in this respect: he found that neighbouring bounce modes further filter the rapid oscillations and allow more accurate predictions (better agreement with the asymptotic technique) for a given grid.

4.6.2. Crosstalk between points on an orbit. Glancing at either of the two asymptotic expressions (20) or (23) reveals that the Fourier amplitudes contain rapidly varying terms (the oscillatory ones) and slowly varying terms (e.g. the $|\Theta''|$ term in the simple expression). This behaviour was already predicted as well as analytically analysed for a simple example in Van Eester (1995): relatively small variations in v or x cause the Fourier amplitude (and the associated RF diffusion coefficient and dielectric response) to oscillate around an average value. An example is depicted in Fig. 4, in which both the full expression (based on the cosine in (20) or (25), the average amplitude of the square of which is $\frac{1}{2}$) and the averaged expression (based

https://doi.org/10.1017/S0022377801001246 Published online by Cambridge University Press

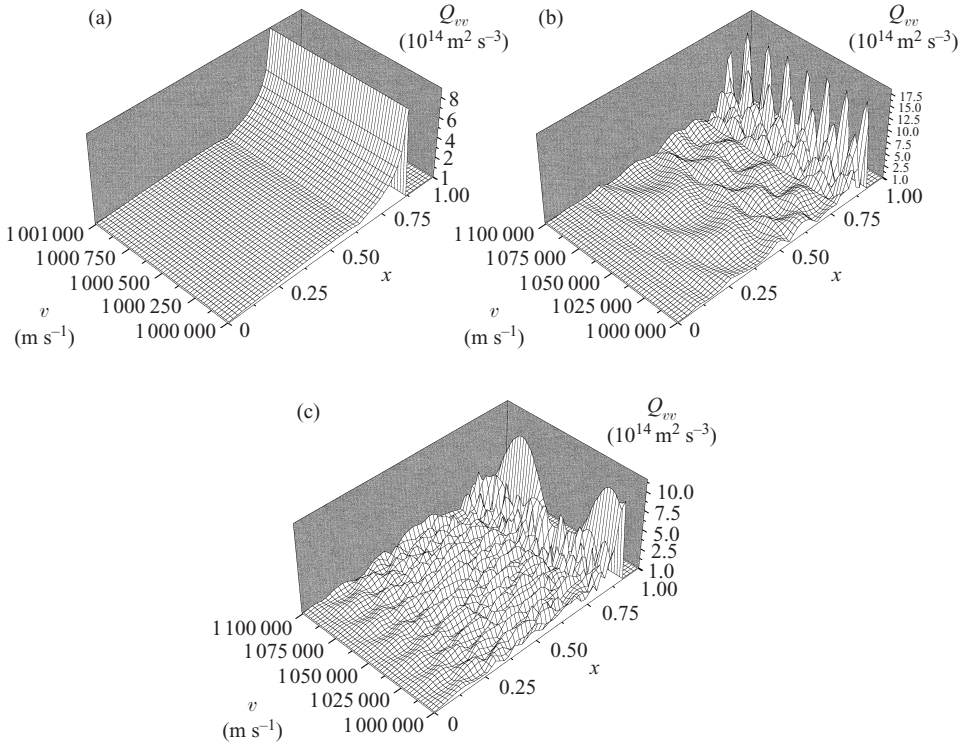

Figure 4. RF diffusion coefficient Q_{vv} for a co-streaming ^{3}He population with velocities ranging from 10^6 to 1.1×10^6 m s^{-1} heated at its fundamental cyclotron frequency in the TEXTOR tokamak. Simple analytical wave field amplitudes are used and uncorrelated resonances are assumed. (a) decorrelated SP points. (b) Correlated SP points. (c) Correlated SP points of the cubic approximation of the phase.

on the sum of the two uncorrelated SP point contributions, involving the square of the absolute value of the exponential, the amplitude of which is 1) are given. Unless the true and approximate turning points lie close to one another, the cubic term in the approximate phase accounted for in (23) causes an unphysical interference pattern on a shorter scale than the actual interference pattern. Note that only a small fraction of the velocity domain was depicted: when highly energetic tails of a few hundreds of kiloelectrovolts are formed, the minimal velocities are small (thermal region) while the maximal velocities to be considered are a few times 10^6 m s^{-1}.

The fine structure observed in the pictures of the diffusion coefficient has severe consequences for the required grid space in case one desires to make a fully rigorous computation. Figure 4 presents an illustration for the TEXTOR case. The major radius $R_0 = 1.75$ m and the magnetic surface has a Shafranov-shifted circular cross-section with radius $r = 0.25$ m. The Shafranov shift of the magnetic axis is 0.07 m. The toroidal mode number $n = +13$, the poloidal mode number is 6 and the radial wave vector component $k_\rho = -30$ m^{-1}. The frequency $f = 25$ MHz, the central toroidal magnetic field $B_0 = 2.6$ T, and the angle between the parallel and the toroidal direction is taken as $\alpha = 0.05$. Figure 4 suggests that it is reasonable to 'coarse-grain' and use the average expressions. This is what was done

https://doi.org/10.1017/S0022377801001246 Published online by Cambridge University Press

in the well-known computation of Stix (1975), in which only one SP point contribution is evaluated and a factor of 2 is used to include the effect of the second SP point. Moreover, Stix considers the local value of the field, leaving the sum on the poloidal modes implicit. Summing on all individual (decoupled) contributions from the individual SP points (omitting the faulty cross-talk between cubic SP points exemplified by the oscillatory behaviour of the asymptotic part of the Airy function expression, which always accounts for two SP points at the time) also seems the most straightforward and computationally appealing approach to generalise to non-up–down-symmetric equilibria. Note that the SA method is slightly altered now: rather than only yielding finite results when the factor $j+\xi_0-k'k_{\max}+\ldots+k''k_{\max}$ is zero, there are extra contributions whenever it is odd.

The physical interpretation of the obtained oscillatory behaviour is straightforward: whether a particle is accelerated or decelerated by an electric field depends on the relative phase of the particle's velocity and of the electric field. Subsequent encounters with resonant layers may either be constructive or destructive. Omitting collisions or any other decorrelation mechanism, the relative phase factor between the two encounters (one above, one below the midplane) with a given resonance determines the correlation between the two energy kicks, i.e. determines the net effect per transit. This relative phase information is embedded in the above asymptotic expressions. Remember that the asymptotic technique is used to make an easy evaluation of the RF response possible but that collisions or decorrelation do *not* enter the computations at this point, except for the fact that causality ensures finite non-zero damping at the resonant bounce mode (see (19)). The most difficult step in the computation (for which the SP, FFT or SA technique is used) involves nothing more than the evaluation of the Fourier components of quantities, and is the consequence of the choice of making a coordinate transformation to coordinates that are more suitable for the (later to be done and much easier) evaluation of the dielectric response. If both the active and reactive terms of the dielectric response are wanted, all Fourier integrals in the bounce spectrum have to be computed. In the present work, only the active terms are looked at, and thus only the resonant bounce mode has to be computed. When decorrelation (e.g. the finiteness of the decorrelation time) is accounted for in a rigorous way, the phase factor will be of importance to determine the net effect of the wave–particle encounters over many transits. With the presently adopted 'causality' decorrelation model (zero decorrelation time with respect to the transit time, infinite decorrelation time with respect to cyclotron time), this relative phase is somewhat superfluous in that it merely causes a local wiggle in the absorption efficiency.

4.6.3. Influence of the orbital topology and of the poloidal magnetic field. An important difference between the diffusion coefficient adopted here and that from a uniform plasma theory is that resonant interaction only occurs if the orbit actually cuts the resonance curve. This is demonstrated in Fig. 5, in which the diffusion coefficient for a given field is depicted for a co-streaming deuterium population $v = 10^6\,\mathrm{m^{-1}\,s}$ in the present JET. The major radius $R_o = 2.9\,\mathrm{m}$, the minor radius is 1 m, the magnetic surfaces are D-shaped with a Shafranov shift of the magnetic axis of 0.065 m, an elongation of 1.7 and a triangularity of 0.21, the poloidal mode number is $m = 6$, the radial wave vector component $k_\rho = -30\,\mathrm{m^{-1}}$, the frequency $f = 25.5\,\mathrm{MHz}$, the central toroidal magnetic field $B_o = 3.7\,\mathrm{T}$, and the angle between the parallel and the toroidal direction is $\alpha = 0.15$ at the outboard side of the

https://doi.org/10.1017/S0022377801001246 Published online by Cambridge University Press

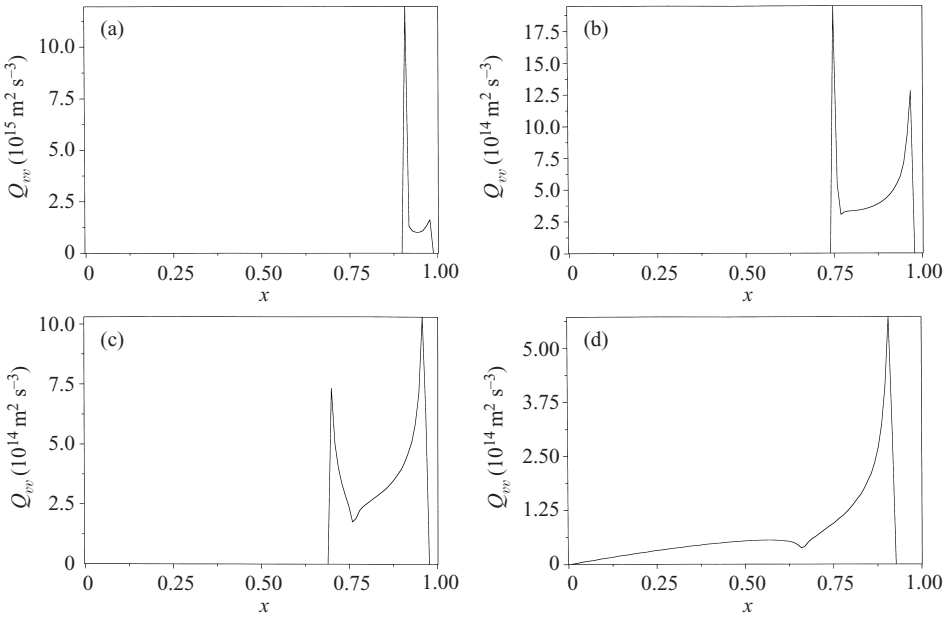

Figure 5. RF diffusion coefficient Q_{vv} for a co-streaming D population with velocity $v = 10^6\,\mathrm{m\,s^{-1}}$ heated at the fundamental cyclotron frequency in the JET tokamak. Simple analytical wave field amplitudes are used and uncorrelated resonances are assumed. (a) $\rho = 0.35\,\mathrm{m}$; (b) 0.39 m; (c) 0.4 m; (d) 0.6 m.

equatorial plane. For the chosen parameters, the non-Doppler-shifted resonance is at 0.03 m to the high-field side of the geometric axis. On surfaces too close to the magnetic axis (e.g. $\rho = 0.2\,\mathrm{m}$), only counter-streaming particles ($v_\parallel < 0$) can absorb wave energy. At more externally situated magnetic surfaces, the co-streaming particles also interact with the wave. First, interaction only occurs in the trapped region, but for increasing ρ the tangent resonance towards the high-field side of the non-Doppler-shifted resonance gradually moves towards the trapped/passing edge. At $\rho = 0.39\,\mathrm{m}$, a small fraction of the co-passing particles contribute to the damping. At $\rho = 0.6\,\mathrm{m}$, all passing particles interact with the field. The efficient heating of particles that have their resonance near the tangent resonance is clearly distinguishable. At the tangent resonance close to the trapped/passing boundary, particles are very efficiently heated.

In a uniform plasma, either a particle is everywhere in resonance with the RF field or it is not resonant at all. Non-uniformity results in varying $v_\parallel, \boldsymbol{\Omega}$ and $k_\parallel$ and confines the resonant cyclotron interaction to discrete points along the orbit. Whereas for a uniform plasma the diffusion is always non-zero for some subclass of particles (notably those that satisfy

$$v_\parallel = v_{\parallel\mathrm{res}} = \frac{\omega - N\boldsymbol{\Omega}}{k_\parallel}$$

for given $\omega, \boldsymbol{\Omega}$ and $k_\parallel$), the orbital topology excludes regions in c.o.m.-space to be eligible for resonant interaction. The transition from the subspace where no damping occurs to that where the resonance condition can be satisfied is not characterized by a simple 'switch-on' Heaviside function behaviour. Making a number of simplifying assumptions (constant $v_\parallel$ near the resonance, circular cross-section, rapid decorrelation), Stix (1975) noted that the diffusion coefficient becomes infinite at

https://doi.org/10.1017/S0022377801001246 Published online by Cambridge University Press

the frontier between the damping and non-damping regions. Adding a more sophisticated description gives rise to a better non-diverging prediction (revealing, for example, that the damping is switched off in a narrow region) but qualitatively adds nothing new. The physical interpretation of the behaviour that Stix observed is straightforward: because the Doppler shift depends on the considered c.o.m., the resonance for varying c.o.m. is satisfied at varying poloidal positions along the orbit. When the resonance approaches the point where it no longer cuts the orbit, the two resonance points lying symmetrically about the midplane move toward the turning point in the midplane at which (provided the SP point condition is satisfied at the turning point) they merge and their velocity component along the major radius goes to zero ($\dot{R} = 0$, i.e. the particle remains in resonance for a long time). Beyond that point, no crossing and thus no damping occurs anymore.

It is not straightforward to relate uniform and non-uniform plasma results, because of the basic difference in orbit topology. Considering an orbit very close to the magnetic axis ensures small variations of the magnetic field, and in that sense mimics the uniform-plasma case in which only 'well-passing' particles with constant $v_\parallel$ exist. 'Off-axis' heating on such a surface (with a non-Doppler-shifted resonance that lies well outside the considered surface) resembles the uniform case in the sense that resonance takes place along a (somewhat broadened) line $v_\parallel = v_{\parallel \mathrm{res}}$ in the passing region, but on-axis heating on this surface (small or zero, $v_{\parallel \mathrm{res}}$, and thus most of the resonant particles are trapped) has no immediate counterpart. On such a surface close to the magnetic axis, the SP point expressions, which formally look like uniform-plasma expressions, are not adequate, since the phase of the RF-induced energy change varies too slowly to ensure that the asymptotic method yields meaningful results (in that case the – less localized – FFT or SA prediction is correct). The other extreme is to consider a surface far away from the magnetic axis. Now the asymptotic methods yield meaningful results and the uniform-plasma intuition is recaptured, but the resonance is fulfilled in a wide region in velocity space, and a non-negligible fraction of the particles are trapped.

The localization of the region in configuration space in which absorption occurs is generally delimited both in x and in v: on a given magnetic surface, only a subset of the Doppler-shifted resonances intersect the orbits. This is more pronounced when one looks at the effect of the RF field on the particles near the magnetic axis for an off-axis heating scenario. Because of the limited extent of the orbit, only a small subcategory of resonant $v_\parallel$ values are physically acceptable. For small v, either no resonant x exist or the width in x of the values for which resonance occurs is large. The larger v is, the narrower is the width. Conversely, for a given x (i.e. for a given equatorial pitch angle), absorption only happens for sufficiently large v, guaranteeing a sufficiently large Doppler shift to move the non-Doppler-shifted resonance (which does not intersect the magnetic surface) to the orbit. For x beyond the tangent resonance, no intersection of the resonance with the orbit exists. The tangent resonance position at the banana tip of trapped particles occurs at a fixed x, independent of the poloidal or toroidal mode number. In contrast to tangent resonance at banana tips, the tangent resonance in the equatorial plane does not necessitate that the parallel velocity cancels. Consequently, for a given x (or v), this tangent resonance takes place at a different v (or x) for a different poloidal or toroidal mode number. Figure 1 demonstrated that the RF diffusion coefficient undergoes violent excursions there. Even having adopted expressions that guarantee that the diffusion coefficient is positive for the usual 'causal' decorrelation does

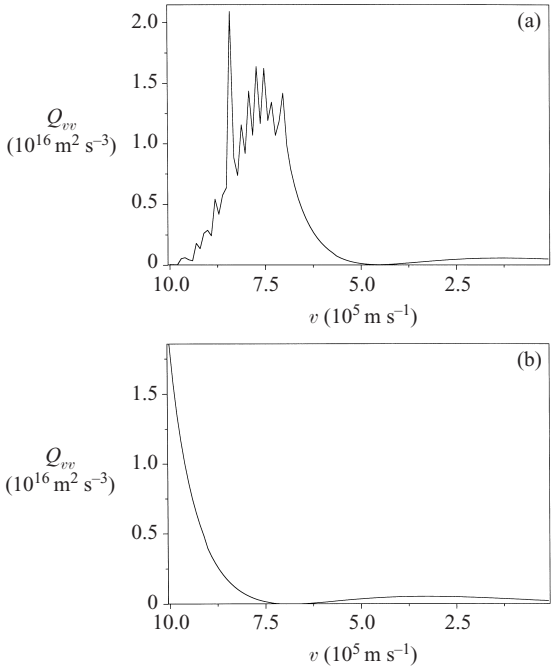

Figure 6. RF diffusion coefficient Q_{vv} for a co-streaming D population with $x = 0.38$ heated at the fundamental cyclotron frequency on the surface $\rho = 0.4$ in the JET tokamak. Simple analytical wave field amplitudes are used, the poloidal mode numbers range from -6 to 6 and uncorrelated resonances are assumed. (a) Standard current (poloidal field), $\alpha_m = 0.15$ m. (b) Reduced current, $\alpha_m = 0.015$ m.

not prevent the coefficient from varying rapidly there. Figure 6 depicts the RF diffusion coefficient Q_{vv} for a case for which the tangent resonance falls inside the region of interest for the co-streaming particles but outside it for the counter-streaming ones. The parameters are those of Fig. 5. Figure 6(a) is for the actual α_m (i.e. for the actual poloidal field magnitude or local plasma current), while Fig. 6(b) shows the result for a reduced current. In the latter case and with the Doppler shift being a function of the plasma current via the parallel wavenumber, much larger velocities are required to arrive at the tangent resonance point than in the case with the normal current. While in the former case some particles benefit from large energy excursions caused by the efficient heating at the tangent resonance, this does not happen in the latter in the depicted velocity region.

Looking at the expression for the Jacobian in (5) and that of the function $\mathscr{B}_N$ in (17), both of which are inversely proportional to the transit frequency, one is induced to overestimate the importance of the tangent resonance in the equatorial plane at the high-field side (where the transit frequency vanishes) compared with that at the low-field side. This dependence on the transit frequency is deceiving, however, since the factor ω_b^2 disappears when all quantities are expressed as functions of time. When that is done, the same major radius velocity factor dR/dt appears and the high- and low-field-side intersections of the magnetic surface with the equatorial plane play an identical role. It is this factor that makes heating at a banana tip efficient. Recall, also, that the simple 'causal' decorrelation used throughout this paper always assumes sufficiently dense spacing of the SP points to always have a resonant mode. Considering a given decorrelation frequency, the

https://doi.org/10.1017/S0022377801001246 Published online by Cambridge University Press

'causal' treatment seems most justified near the turning point, since the transit frequency goes to zero there, which guarantees that many terms contribute to the resonant interaction ('dense' set of contributions in (19)). On the other hand, the fact that many bounce modes resonantly interact with the particles (*at most* one bounce mode of which has a SP point for which the actual turning point and the 'cubic' one coincide) shows that the contribution associated with the true turning point is less pronounced than the naive application of the causal treatment (which – because of the assumed continuous bounce mode SP point density always yields a resonant interaction if the orbit intersects the resonance curve) suggests.

The coordinate transformation is deceiving in a second way: particles seem to be bunching at the trapped/passing edge, since the Jacobian is inversely proportional to the transit frequency, and so for a plasma in thermodynamical equilibrium (Maxwellian), the local density distribution JF_0 seems to peak there. This is to be expected, however: because of the particle trapping, all particles cross the low-field-side equatorial point (where their parallel velocity is maximal) while only the passing ones cross the high-field-side point. Transforming to the local velocity components in a given infinitesimal volume involves transforming the elementary angle $d\Phi_b$ into the poloidal angle $d\theta = (d\theta/dt)(dt/d\Phi_b)\, d\Phi_b$. The factor that appears ensures that regions where the poloidal velocity is higher than the average poloidal velocity cover a larger poloidal domain than regions where the velocity is low. As a result, the same number of particles reside in each infinitesimal box. The usual local expression for the density (independent of the poloidal angle) emerges, as it should.

4.6.4. Crosstalk between modes in the wave spectrum. On Fig. 6, one can see that the RF diffusion coefficient, and the associated heating, goes to zero near $v = 4 \times 10^5\,\mathrm{ms}^{-1}$ (a) and $v = 7 \times 10^5\,\mathrm{ms}^{-1}$ (b). The reason for this is not the familiar finite-Larmor-radius effect associated with the zeros of the Bessel functions in the Kennel–Engelman operator, but an effect that is absent in uniform plasma theory: owing to the presence of the multiple poloidal harmonics of the electric field, independent poloidal modes can constructively or destructively interact with one another. This again is an effect that is in agreement with physical intuition: the particle will be accelerated or decelerated, depending on the relative phase of its velocity and that of the total electric field. Some poloidal modes may be in phase with the particle velocity, while others are in phase opposition. One would intuitively expect that the terms corresponding to interference average out to give a zero contribution. This is indeed formally the case. There is a subtlety, however. This becomes clear when we look at the combined effect of two of the poloidal modes. We start from the Fourier amplitude of the field, and subsequently express the term corresponding to the second poloidal mode (evaluated at the SP point of this mode) in terms of quantities related to the first SP point using a Taylor series expansion (we assume that we are away from the turning point and that the poloidal modes are not too different, so that the Taylor series can be truncated after the linear term). We can then write

$$\left|\sum_m \mathscr{L}_{(m)} e^{i[m\theta(\Phi_b)+n\varphi(\Phi_b)-N\phi(\Phi_b)}\right|^2 = \left|\sum_m \mathscr{L}_{(m)} e^{i[m\theta(\Phi_b)+H(\Phi_b)}\right|^2$$

$$\approx \left|e^{i[m_1\theta(\Phi_{b_1})+H(\Phi_{b_1})}\right|^2 \left|\mathscr{L}_{(m_1)} + \sum_{m\neq m_1} \mathscr{L}_{(m)} e^{i[(m-m_1)g(\Phi_{b_1})}\right|^2, \qquad (27)$$

https://doi.org/10.1017/S0022377801001246 Published online by Cambridge University Press

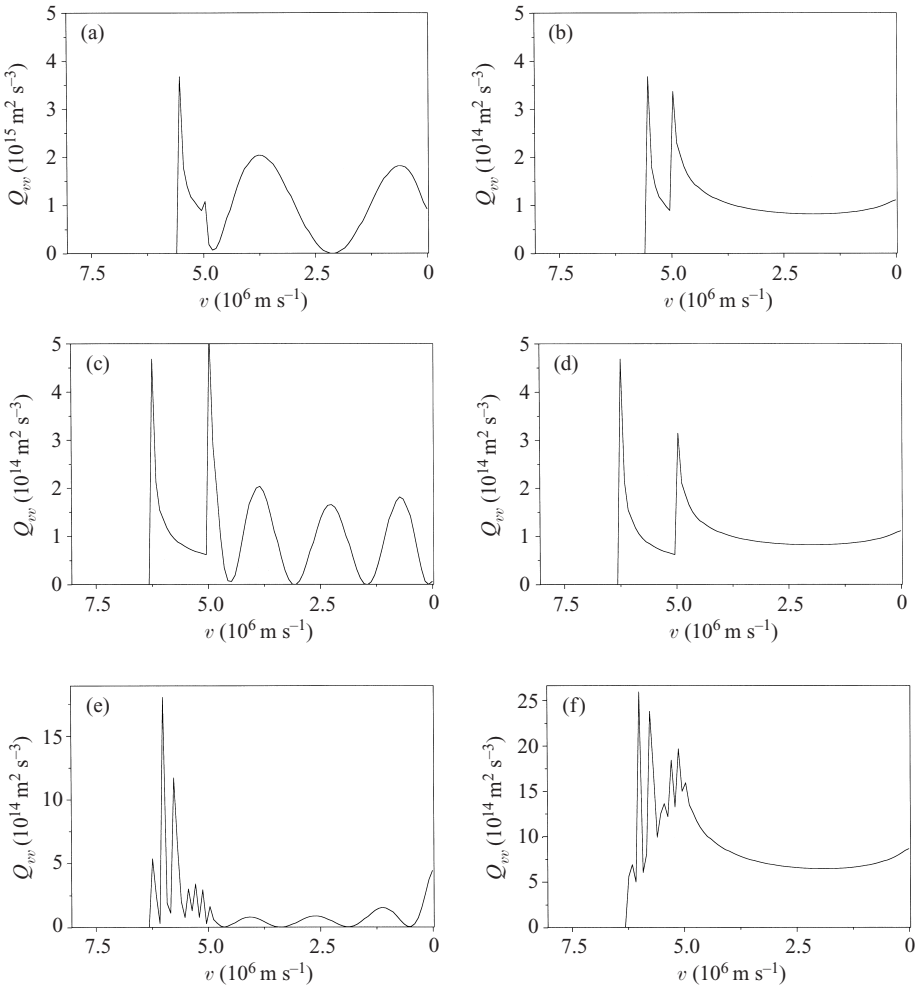

Figure 7. RF diffusion coefficient Q_{vv} for a counter-streaming D population heated at its fundamental cyclotron layer in JET: (a,b) $m = 0$ and $m = 6$; (c,d) $m = 6$ and $m = +6$; (e,f) m ranges from -6 to $+6$; (a,c,e) actual wave phase (correlated modes); (b,d,f) no phase information (decoupled modes).

which, for two poloidal modes, is a sum of four terms, two of which are positive-definite and represent the decoupled contribution of the individual poloidal modes. The other two terms oscillate around this average. To a good approximation, the second term in the phase of the exponential is negligible with respect to the first. It is, however, important to note that, expressed in terms of one of the independent variables (e.g. the velocity), the phase of this oscillating term varies by 2π (full period) when the velocity changes by

$$\Delta v \approx \frac{2\pi}{(m - m_1)\,\partial g/\partial v}, \qquad g(\Phi_b) \approx \theta(\Phi_b) - \frac{R(\Phi_b)}{dR/d\theta|_{(\Phi_b)}}.$$

This interval is large when the SP point varies slowly with v, or when the considered poloidal modes do not differ much. This is clearly demonstrated in Fig. 7, in which both the total sum and the sum of the individual decoupled contributions are

https://doi.org/10.1017/S0022377801001246 Published online by Cambridge University Press

plotted for (a,b) two neighbouring modes (m = 0 or 6) and (c,d) two more distant modes (m = −6 and +6) and for a wide velocity range. The plots (a), (c) and (e) are for the actual field, while the coupling terms are omitted in (b), (d) and (e). The parameters are those of Fig. 5 and ρ = 0.4 m. In the case corresponding to Fig. 7(c,d), 'coarse-graining' by omitting the oscillatory behaviour may still crudely be justified; in the former it is already more questionable. The last figures (e,f) presents the result for a total of 13 modes, and show that approximating the effect of the total field by the effect of the individual modes locally in velocity space overestimates the RF diffusion and local damping by a factor of 4–8! The conclusion that one has to draw from this exercise is that adopting simplified wave profiles may lead to erroneous predictions for the absorption efficiency. Whereas 'coarse-graining' commonly makes sense when looking at the combined effect of different resonances because of a sufficiently fast collision-related decorrelation (see Figure 4), such procedure has to be avoided when evaluating the local heating efficiency.

4.7. Summary

The results of Sections 4.1–4.6 can be summarized as follows:

1. The general formulae for the dielectric response proposed by Kaufman guarantee positivity of the absorbed power for Maxwellian plasmas for any wave mode and particle orbit. Approximate expressions based on asymptotic techniques lose this important characteristic.
2. Asymptotic techniques may nevertheless be used in many cases to compute the Fourier amplitudes of the RF-induced energy change needed for the evaluation of the response and in particular the absorption. When asymptotic techniques fail, FFT or SA methods or even direct numerical integration yields the needed coefficients.
3. Asymptotic techniques clearly show the effect of the constructive/destructive interference of various energy kicks on a single transit. Some of the obtained fine structure has a physical origin (Fig. 4b) while some is an artefact of the adopted model (Fig. 4c). Using the simplest possible ('causal') decorrelation, one can distinguish three regimes:
   (a) When the decorrelation time is fast compared with the bounce time but slow compared with the cyclotron time scale, the various resonances along the orbit are decoupled and the total energy change is the sum of the kicks the particle receives at the individual resonances. Changing the decorrelation time does not change the net absorption rate.
   (b) When the decorrelation time is slow compared with the bounce time, many resonant interactions have to be accounted for and the relative phase of the RF-induced energy change between resonances matters. This second regime is known as the superadiabatic regime. Except for a limited set of orbit parameters, the net energy change is zero.
   (c) The final regime is that where the decorrelation time is of the order of the bounce time. The details of the decorrelation model now critically distinguish between efficient and inefficient absorption for a given electric field.
4. The first of the above-mentioned cases (fast decorrelation) is the one that is relevant for particle populations that are not too energetic. It yields formulae that bear close resemblance to those of the uniform plasma, but, unlike the

uniform case, the nomenclature 'collisionless' is misplaced, since collisions – or some other decorrelation mechanisms – are a necessary ingredient of the model. For this case, the interference is so fine-structured that it is of secondary importance and can be neglected (minuscule variations in one of the parameters can significantly change the phase, and so the detailed phase information loses its meaning while the average – much less fine-structured – response is what eventually matters).

5. The inferference associated with the different phasings of the various poloidal and toroidal modes in the wave spectrum has to be accounted for to get a realistic prediction of the absorption efficiency for a given field: it is not sufficient to account only for the local wave amplitude or for an average wave amplitude on an orbit to make a reasonable prediction of the heating efficiency for a given field.

Until now, only the local values of the RF response for given x and v have been computed. In the weak Galerkin form of the Fokker–Planck equation, suitable for finite-element treatment, integrals of this response over small domains appear. The simplest possible way to provide the needed information is to rely on the fact that the basis functions vary on a much shorter scale than the coefficients and to approximate the required integrals by the value of the coefficient at the centre point of the element multiplied by the analytical integral of products of the basis functions. Better approximations can be provided by relying on interpolation schemes, using a truncated Taylor series expansions of the required integrand and analytically obtaining a better approximation of the integral. Some useful expressions can be found in Prudnikov et al. (1986).

4.8. Note on finite-banana-width effects

Although the general theory due to Kaufman allows for it, the present paper does not account for finite-banana-width effects, i.e. it assumes that guiding centres are confined to magnetic surfaces. One of the consequences of this approximation is that RF-induced transport is neglected and that the Fokker–Planck equation is a partial differential equation with only two independent variables. Computationally, this has a clear advantage, since it requires less computer time and memory, but physically it decouples in a somewhat artificial way the radial transport from the diffusion in velocity space. The full (3D) resolution of the Fokker–Planck equation is, at least formally, not more difficult than that of its 2D counterpart but it requires enhanced bookkeeping in practice. The first step is the computation of expressions for the Fourier coefficients of the RF-induced temporal change of the energy on a grid of $\mathbf{\Lambda}$. The toroidal angular momentum P now appears instead of the flux Ψ as one of the variables. The obtained expressions require the relation between the 3D guiding-centre position, the $\mathbf{\Lambda}$ and the bounce angle to be known. An analytical expression for the bounce-angle dependence along an orbit is not available in general, but one can rely on numerical integration to find it (as is routinely done when solving the diffusion equation using the Monte Carlo approach). Formally, the expressions for the building blocks are identical to those presented earlier in this section.

5. The collision operator

Since, by construction, the slowly varying distribution function does not depend on any of the short-time-scale variables $\mathbf{\Phi}$, removing all short-time-scale dependence

https://doi.org/10.1017/S0022377801001246 Published online by Cambridge University Press

from the collision term in the Fokker–Planck equation only requires performing a bounce average of the coefficients of the collision operator. When P is approximated by Ψ and when the background on which the examined species collisionally relax is assumed to be in thermodynamic equilibrium, the result is formally identical to the uniform plasma expression except that the coefficient $v_\parallel^2/v_\perp^2$ in the expression for the S_x flux is now bounce-averaged:

$$\left.\frac{\partial F_0}{\partial t}\right|_{\text{collisions}} = \frac{1}{J}\left\{\frac{\partial}{\partial v}\left[J\left(D_{vv}\frac{\partial F_0}{\partial v} - F_v F_0\right)\right] + \frac{\partial}{\partial x}\left(J\left\{D_{\Phi\Phi}\left(\frac{2x}{v}\right)^2\left\langle\frac{v_\parallel^2}{v_\perp^2}\right\rangle\frac{\partial F_0}{\partial x}\right\}\right)\right\}. \tag{28}$$

The expressions for D_{vv}, F_v and $D_{\Phi\Phi}$ (where Φ is the pitch angle) can be found, for example, in Karney (1986). Since the collision operator is written as the divergence of a flux, the corresponding term in the weak Galerkin form of the Fokker–Planck equation is

$$\int d\mathbf{\Lambda}\, JG\left.\frac{\partial F_0}{\partial t}\right|_{\text{collisions}} = -\int d\mathbf{\Lambda}\, J\left\{\frac{\partial G}{\partial v}\left(D_{vv}\frac{\partial F_0}{\partial v} - F_v F_0\right) + \frac{\partial G}{\partial x}\left[D_{\Phi\Phi}\left(\frac{2x}{v}\right)^2\left\langle\frac{v_\parallel^2}{v_\perp^2}\right\rangle\frac{\partial F_0}{\partial x}\right]\right\}. \tag{29}$$

The surface terms are not trivially zero, but do not appear at the internal boundaries of the finite elements in the final equations when choosing basis functions that are sufficiently smooth to guarantee the – physical – continuity of the flux between neighbouring finite elements. As boundary conditions at the edges of the integration domain, the fluxes are required to be zero. This prevents particles to escape from or enter the considered region, i.e. it ensures conservation of the total number of particles.

6. Comments on the weak form of the Galerkin formalism

The Fokker–Planck equation is solved using the finite-element method. Since this method is well known, only a short sketch of the practical implementation is given. Continuity of the integrated flux across finite-element boundaries is ensured numerically by a proper choice of the basis functions. In each finite element $[v_i, v_{i+1}] \times [x_j, x_{j+1}]$, the adopted 2D basis functions are of the form

$$G_{ij}^{\alpha}(v,x) = H^{\beta}\left(\frac{v - v_i}{\Delta_v}\right)H^{\chi}\left(\frac{x - x_j}{\Delta_x}\right), \tag{30a}$$

in which the functions $H^i(\xi)$ satisfy

$$H^1|_{\xi=0} = \left.\frac{dH^2}{d\xi}\right|_{\xi=0} = H^3|_{\xi=1} = \left.\frac{dH^4}{d\xi}\right|_{\xi=1} = 1, \tag{30b}$$

while all other values of either the functions or their derivatives are zero at both boundaries. Approximating F_0 by a polynomial of order three in each finite element, F_0 can be written as $\mathbf{f}_{ij}^T \cdot \mathbf{G}_{ij}$, and so the Fokker–Planck equation, after projection

https://doi.org/10.1017/S0022377801001246 Published online by Cambridge University Press

on the 16 basis functions $G = \mathbf{g}_{ij}^T \cdot \mathbf{G}_{ij}$, reduces to the local linear 16×16 system

$$\mathbf{g}_{ij}^T \cdot \hat{\mathbf{S}} \cdot \mathbf{s}_{ij} = \mathbf{g}_{ij}^T \cdot (\hat{\mathscr{Q}} + \hat{\mathscr{C}} + \hat{\mathbf{L}}) \cdot \mathbf{f}_{0ij} \tag{31}$$

in which the elementary $\hat{\mathbf{S}}$, $\hat{\mathscr{Q}}$, $\hat{\mathscr{C}}$ and $\hat{\mathbf{L}}$ are matrices of integrals of products of two basis functions multiplied by a function $\mathscr{M}$ of v and x. These integrals can be evaluated in various ways:

(a) using a 2D Gaussian integration scheme, which yields correct results for polynomial functions $\mathscr{M}$ of up to order three both in v and x;

(b) using analytical expressions while approximating the coefficients by low-order polynomials; or simply

(c) dropping the variation of the coefficients and just analytically integrating the products of base function.

Note that when the 2-element basis functions

$$H^{\beta}\left(\frac{v - v_i}{\Delta_v}\right)\left[H^{\chi}\left(\frac{x - x_j}{\Delta_x}\right) + H^{\chi+2}\left(\frac{x - x_{j-1}}{\Delta_x}\right)\right]$$

with $\chi = 1$ or 2 are used, the basis functions and their derivatives are continuous inside the finite element as well as across the finite-element boundary line connecting the neighbouring elements (v_i, x_j) and (v_i, x_{j-1}). Projecting onto these two-element basis functions thus results in the exact cancellation of the left surface term in elements j by the right one in $j - 1$. Choosing lower-order basis elements that are continuous in the element but that do not guarantee continuity of all derivatives in the basis functions can be taken as well, provided that it is possible to install numerical jumps in the surface terms to guarantee that the physical flux itself is nonetheless continuous. Assembling all the local systems into a large linear system by combining them pair-wise to emulate such 2-element base functions, leads to four sets of overlapping 4×4 sub-blocks. The global linear system thus has a limited bandwidth and can be solved using standard banded-matrix inversion routines

7. Solving the Fokker–Planck equation: two small examples

As practical examples, the JET (D)–T fundamental cyclotron heating scenario and the combined NBI+RF heated (^{3}He)–(H)–D scenario of TEXTOR will now be discussed briefly. The aim of the presented examples is to provide an illustration showing the sensitivity of the predictions on the details of the considered model, and to provide an idea of the scenarios that can be modelled with the BATCH code. No attempt has been made to capture the full physics: although the particles feel the effect of the total electric field and notwithstanding the fact that the toroidal and the poloidal spectra contain about 60 modes (in the case where the field structure is essentially that of a fast wave – many more in the case where the Bernstein wave plays a role), only 1 toroidal mode and a limited number of poloidal modes are retained. Furthermore, the electric field was evaluated for Maxwellian species rather than being computed iteratively to self-consistently account for the non-Maxwellian distribution. The electric field computations have been performed using the present CYRANO code, which retains all three electric field components and allows one to study minority fundamental cyclotron heating scenarios. The BATCH Fokker–Planck code uses bidimensional cubic basis functions in the finite elements.

https://doi.org/10.1017/S0022377801001246 Published online by Cambridge University Press

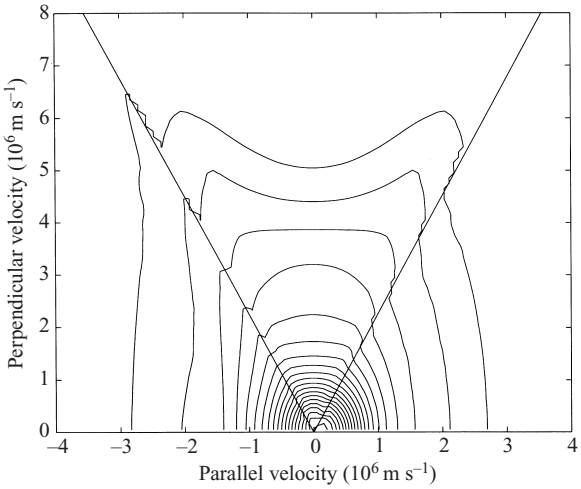

Figure 8. Distribution function of a D population heated by central fundamental cyclotron heating in JET. The lines are level lines with levels $jF_{0,\max}/20(j = 0, \ldots, 19)$ between the maximum value $F_{0,\max}$ in the thermal region and the minimum $F_{0,\min} = 0$ in the large-velocity region. The thermal velocity $(kT/m)^{1/2}$ of the background ions is 4.3×10^5 m s^{-1}.

For standard runs, 60 elements are used in both the velocity and the x direction. The velocity domain is subdivided into two parts: in the region close to $v = 0$, a rather fine grid spacing is used to capture the thermalization process. In the remaining velocity region, a coarser grid is taken. Likewise the co- and counter-streaming particles are each modeled by 30 finite elements, 15 of which are taken in the passing and 15 in the trapped region. In each subinterval, uniform grid spacing is used. Remembering the fine structure of the RF diffusion coefficient near the trapped/passing edge (see e.g. Fig. 7e), the adopted grid dimensions may be marginal, and thus the results obtained here should be considered as indicative only. Their only purpose is to illustrate the sensitivity of the obtained solutions to the details of the RF diffusion operator.

The parameters for the JET case are as follows. The central density is 5×10^{19} m^{-3}, the edge density is 5×10^{18} m^{-3}, and the density profile factor is 0.01. The central temperatures are 7.3 keV and 6.6 keV for electrons and ions, respectively. The temperature profile factor is 2. The toroidal magnetic field strength $B_0 = 3.7$ T, the total plasma current is 3.3 MA and the current density profile factor is 3. The magnetic shift is 0.065 m, the elongation is 1.7 and the triangularity is 0.21. These data are typical for shot number 43015 during the D–T campaign at JET. A minority D concentration of 9% is taken. The generator frequency is 28 MHz and only one toroidal mode will be considered: $n = 28$. The non-Doppler shifted resonance lies at the geometric centre, 0.065 m on the high-field side from the magnetic axis.

The adopted parameters correspond to central fundamental cyclotron heating of the deuterium minority. Figure 8 shows the distribution function at $\rho = 0.26$ m. The actual local phase of the electric field is used. The figure shows a contour plot of the distribution in the equatorial plane expressed in function of the local parallel and perpendicular velocities corresponding to the independent variables v and x with which the actual computation was done. A total of 20 contour lines, equally spaced between the highest and lowest value of the distribution, is used. In the

https://doi.org/10.1017/S0022377801001246 Published online by Cambridge University Press

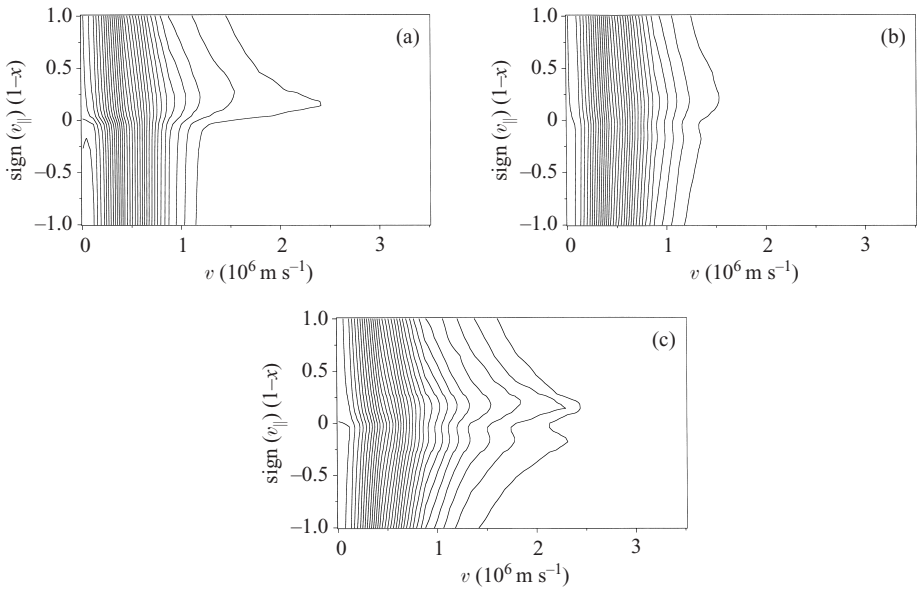

Figure 9. Level lines of the distribution function for off-axis heating of a D minority in JET accounting for (a) the actual local electric field, (b) the amplitudes of the poloidal components of the electric field but not the associated phase, and (c) the total amplitude of the field. The thermal velocity $(kT/m)^{1/2}$ of the background ions is 3.4×10^5 m s^{-1}. Trapped orbits are decoupled into two passing orbits.

thermal region a slightly deformed Maxwellian is found (for a Maxwellian, the contour lines are circles). This is what one expects for a minority heating regime for which, for a given constant electric field, the RF diffusion coefficient is maximal in the thermal region (zeroth-order Bessel function in front of the electric field component rotating with the ions in the Kennel–Engelmann operator). Note also that the co- and counter-streaming particles are not heated with the same efficiency: the counter-streaming particles reach higher velocities than their co-streaming counterparts. The two straight lines indicate the trapped/passing boundary. In the trapped region, the typical 'rabbit-ear' distribution function is observed, the 'ears' of the rabbit corresponding to the tangent resonance at the banana tips where efficient heating takes place (for an elegant analytical treatment, see e.g. Chang and Colestock 1990). The ears are only well pronounced at high velocities. At lower velocities, the RF heating is also present, but more frequent Coulomb collisions make the distribution more isotropic. For the adopted field, the RF power density on the surface $\rho = 0.26$ m is 0.42 MW m^{-3} and the average energy of the population is 185 keV (i.e. the effective temperature is 122 keV).

To illustrate the importance of retaining the details of the electric field, Fig. 9 depicts the obtained distribution function at $\rho = 0.5$ m for the same field but lowering the frequency to 25 MHz (off-axis heating) and making three different approximations. The figure shows the contour lines of the minority distribution, maximal in the small-v ('thermal') region and exhibiting more or less energetic tails (position of the contour line corresponding to the lowest F_0 level). In all figures, 33 contour lines are drawn. The contour lines in Fig. 9(a) depict the result when the actual field structure is considered. Figure 9(b) gives the result when only the amplitudes of the various components is accounted for but the actual phase information is omitted

https://doi.org/10.1017/S0022377801001246 Published online by Cambridge University Press

(see (27)). Figure 9(c) finally shows the result when only one electric field component having the amplitude of the total field but having $m = 0$ (poloidal dependence of the field and role of the poloidal field omitted) is considered. All three results agree on which population is most affected by the heating: the particles streaming in the same direction as the magnetic field. This is what one would intuitively expect from a one-dimensional reasoning: the field amplitude of a fast wave (for which the electromagnetic flux dominates the kinetic flux) is large when the wave in undamped (flux maximal), and its amplitude decreases when it propagates further away from the antenna and penetrates deeper into the damping zone. Consequently, particles with a large, positive Doppler shift resonantly interact with a larger field than particles whose Doppler shift is small or negative. Since the toroidal motion dominates the Doppler shift unless m is large or near the magnetic axis, co-streaming particles fall in the first and counter-streaming ones in the second category. The effect of the poloidal magnetic field is clear when one compares Fig. 9(c) with the other two cases: accounting for the finite poloidal field (cases (a) and (b)) suppresses the absorption of the counter-streaming particles. Neglecting the phasing between the various poloidal components further accentuates this difference: In (a), the formation of an asymmetric tail is most clearly observed. In (b), it is less clear, since both the co- and counter-streaming populations are less affected than in (c). The RF power densities equally reflect the effect: omitting all poloidal details yields an RF power density of $0.22\,\mathrm{MW\,m^{-3}}$ and an average energy of 26 keV. Fully including the poloidal non-uniformity yields an RF power density of $0.15\,\mathrm{MW\,m^{-3}}$ and an energy of 18 keV. Only accounting for the various amplitudes of the poloidal components but omitting the interference gives the lowest estimate for the RF power density ($0.12\,\mathrm{MW\,m^{-3}}$) and average energy (12 keV).

TEXTOR can be heated using neutral-beam injection and/or RF heating. In TEXTOR, the plasma current is antiparallel to the magnetic field, and thus a co/counter-beam is fired antiparallel/parallel to the direction of the current. It was observed experimentally that synergistic effects occur on combining both heating methods. This effect is due to the fact that the beam ions are highly energetic and thus weakly collisional, which renders the RF heating more efficient for a given RF power level. A collective Thomson scattering diagnostic is being installed on TEXTOR. It will provide experimental information on what the distribution function of the energetic particles looks like (Bindslev et al. 1999). A preliminary theoretical prediction, based on a simplified electric field, is given in Fig. 10. It shows the distribution function of a counter-injected ^{3}He beam heated at its fundamental cyclotron frequency on a magnetic surface close to the magnetic axis ($\rho = 0.11$ m). The parameters for this TEXTOR scenario are as follows. The central density is $5.2 \times 10^{19}\,\mathrm{m^{-3}}$, the edge density is $5.2 \times 10^{17}\,\mathrm{m^{-3}}$ and the density profile factor is 0.7. The central temperatures are 1.55 keV for both electrons and ions. The temperature profile factor is 3.3. The plasma consists of a majority of 65% deuterium and a minority of 15% hydrogen. The toroidal magnetic field strength $B_0 = 2.6$ T, the total plasma current is 0.3 MA and the current density profile factor is 4.95. The magnetic shift is 0.07 m, the elongation is 1.0 and the triangularity is 0. The generator frequency is assumed to be 25 MHz and only one toroidal mode will be considered: $n = 13$. The total power launched is 400 kW. It is mainly absorbed in the central region ($\rho < 0.15$–0.20 m). In Fig. 10, one can clearly recognize the maximum near the injection velocity corresponding to 40 keV (c.f. Gaffey (1976), in which an analytical expression for the distribution function of a beam can be found)

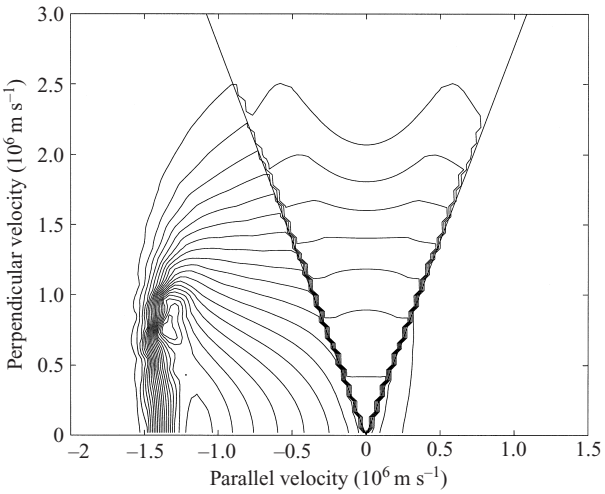

Figure 10. Level lines of the distribution function for a ^{3}He beam injected into TEXTOR and heated at its fundamental cyclotron frequency. The thermal velocity $(kT/m)^{1/2}$ of the background ions is 3.5×10^5 m s^{-1}

as well as the typical 'rabbit-ear' distribution function resulting from efficient RF heating near the tangent resonance at the banana tips of the trapped particles. In TEXTOR, the slowing-down time is small (a few tens of milliseconds), and thus the thermalized population dominates over that of the energetic particles. To remove the thermalized part from the distribution, the collision operator proposed by Gaffey was used when solving the Fokker–Planck equation. This operator rigorously models the collisions when the velocity lies in between the thermal velocities of the ions and the electrons, but fails to describe the thermal region and has a sink at $v = 0$. The average energy of the particle beam depicted in Fig. 10 is 40 keV and the local RF power density is 0.5 MW m^{-3}.

The BATCH code is still under development and further improvement. The results presented here were computed on a Macintosh computer. The variational principle on which the code is based allows to write down the particle number and power balance upon replacing the test function by 1 and by the energy, respectively. Although the power and particle balance associated with the Fokker–Planck equation were satisfied for each of the cases (showing that the linear system is solved satisfactorily), the solutions of the Fokker–Planck equation discussed above should only be considered indicative, since memory and speed limitations rather than rigorous convergence testing of the physical solution dictated the adopted grid size. Some of the fine structure may not be captured appropriately. Initial benchmarking was done by reproducing a number of distributions for situations for which analytical solutions exist: using the full collision operator, a Maxwellian distribution with the proper effective temperature was found in the absence of auxiliary heating. Adopting-the simplified collision operator appropriate for energetic ion beams (Gaffey 1976), the slowing-down distribution function for an 'isotropic' beam was reproduced. For an anisotropic beam, there was qualitative agreement, but the orbital topology included in the code and not in Gaffey's analytical expression (in particular the trapped/passing edge) distinguish the solution found by BATCH from that found by Gaffey.

8. Conclusions

Starting from a formalism due to Kaufman (1972), a model allowing a fully self-consistent treatment of RF heating in toroidal geometry has been formulated (see e.g. Lamalle (1997, 1998) and Van Eester (1995, 1998), and references therein, for details of the wave equation and the Fokker–Planck equations, respectively). It relies on the evaluation of elementary 'building blocks' shared by the wave and Fokker–Planck equations and independent of the distribution function and the actual electric field pattern. The sophistication of these building blocks (describing the interaction between a guiding centre and a wave polarization) determines the sophistication of the description, but their shared use always guarantees that the wave and Fokker–Planck equations are treated on a common footing and are solved self-consistently.

Relying on asymptotic techniques, approximate expressions can be found for the dielectric response and the RF diffusion operator. These expressions bear close resemblance to uniform-plasma formulae, and, although they are not always valid, allow one to gain insight into the impact of the non-Maxwellian character of the distribution function on the propagation and absorption of externally launched waves, and in the role played by the electric field profile in setting up the slowly varying distribution function. When asymptotic methods fail, the FFT method and a semi-analytical technique are available to evaluate the building blocks describing the particle-field interaction.

Various available methods for evaluating the building blocks have been discussed. The equivalence of all methods in regions where they are all valid has been demonstrated numerically. In the case of electron Landau or TTMP damping, the resonance is noticeably less localized than the asymptotic result predicts. A detailed study is made of the performance of various asymptotic expressions. It has been shown that the more detailed stationary-phase method commonly proposed for modelling cyclotron interaction near turning points gives rise to unphysical interference.

In the past, the effect of the tokamak geometry has not always been accounted for in a rigorous way. In this paper, a number of aspects of a more rigorous accounting of the tokamak geometry have been identified and discussed. The variation of the parallel and perpendicular velocity along particle orbits is accounted for, but finite-banana-width effects are omitted.

1. The essentially collisional character of a 'collisionless' tokamak heating scheme has been discussed. It restores the intuition that an electric field does not necessarily accelerate a particle and recalls the hidden but important role of decorrelation: the assumption that the decorrelation is slow on the cyclotron but fast on the diffusion time scale usually made in plasma physics is essential in order to have net RF heating.
2. It has been shown how the orbital topology and the poloidal magnetic field strength influence the RF heating efficiency through the Doppler shift. In a uniform plasma, only particles with the well-defined parallel velocity $(\omega - N\Omega)/k_{||}$ benefit from RF heating. In a non-uniform plasma, the magnitude of the poloidal field and the extent of the orbit determines whether or not a particle is heated. Resonant wave–particle interaction occurs in a band rather than along a single line in configuration space.
3. The role of the constructive or destructive interference of resonances related

to the same resonance condition can usually (at least for the just-mentioned decorrelation time) be omitted using a 'coarse-graining' procedure, avoiding the need to use unpractically fine grids to solve the Fokker–Planck equation numerically. Once again, the intuitive picture that, in absence of decorrelation, the net effect of multiple resonance crossings along an orbit does not trivially lead to heating is recaptured.

4. Finally, the interference caused by the contributions of the individual modes of the poloidal wave spectrum is retained and the effect discussed. Here again, one sees that the intuitive picture of particle heating by an electric field is violated when in practical computations simplifying assumptions are unjustifiably made. In contrast to the previous situation, 'coarse-graining' (often used to avoid having to account for the details of the wave structure in the Fokker–Planck computations) is *not* permitted here, i.e. the actual local electric field has to be accounted for when computing the net effect that RF heating has on a population. An example discussed in the text indicates that the constructive or destructive interference of the various wave components can modify the RF diffusion, and thus the heating, by an order of magnitude. These interference effects cannot be dismissed, so the Fokker–Planck equation should be solved accounting for the local value of the wave phase and not just accounting for its local or surface or orbit averaged magnitude.

The BATCH (Bounce-Averaged Tool for Cyclotron Heating) Fokker–Planck code accounts for the physics in the various expressions discussed in this paper. It evaluates the distribution function for a population heated by RF and/or neutral-beam-injection heating. It uses the complex Fourier amplitudes of the wave field to account for the local electric field value sensed by the particle. At present one toroidal mode and a limited set of poloidal modes only are considered. RF-induced particle transport across magnetic surfaces is neglected, since the Fokker–Planck equation is solved in the zero-banana-width limit (with guiding centres staying on magnetic surfaces). A few preliminary examples have been discussed.

Acknowledgements

I am indebted to Dr P. U. Lamalle and N. Pieret for providing me with the electric field input required for the Fokker–Planck computations.

Appendix A. The magnetic topology and associated coordinate choice

Starting from an arbitrary radial variable ψ and an arbitrary poloidal angle θ, but adopting the standard toroidal angle φ, one can write the co- and contravariant basis vectors and the components of the metric tensor as

$$\mathbf{g}^1 = \boldsymbol{\nabla}\psi, \qquad \mathbf{g}_1 = J_{\psi\theta\varphi}\boldsymbol{\nabla}\theta \times \boldsymbol{\nabla}\varphi, \qquad \boldsymbol{\nabla}\psi = \frac{\partial\psi}{\partial R}\mathbf{e}_R + \frac{\partial\psi}{\partial Z}\mathbf{e}_Z,$$

$$\mathbf{g}^2 = \boldsymbol{\nabla}\theta, \qquad \mathbf{g}_2 = J_{\psi\theta\varphi}\boldsymbol{\nabla}\varphi \times \boldsymbol{\nabla}\psi, \qquad \boldsymbol{\nabla}\theta = \frac{\partial\theta}{\partial R}\mathbf{e}_R + \frac{\partial\theta}{\partial Z}\mathbf{e}_Z,$$

$$\mathbf{g}^3 = \boldsymbol{\nabla}\varphi = \frac{1}{R}\mathbf{e}_\varphi, \qquad \mathbf{g}_3 = J_{\psi\theta\varphi}\boldsymbol{\nabla}\psi \times \boldsymbol{\nabla}\theta = R\mathbf{e}_\varphi,$$

https://doi.org/10.1017/S0022377801001246 Published online by Cambridge University Press

$$g^{13} = g^{31} = g^{23} = g^{32} = 0, \qquad g_{11} = J^2_{\psi\theta\varphi}\frac{|\nabla\theta|^2}{R^2},$$

$$g^{33} = \nabla\varphi\cdot\nabla\varphi = |\nabla\varphi|^2 = \frac{1}{R^2}, \qquad g_{12} = -J^2_{\psi\theta\varphi}\frac{\nabla\psi\cdot\nabla\theta}{R^2},$$

$$g_{13} = g_{31} = g_{23} = g_{32} = 0, \qquad g_{22} = J^2_{\psi\theta\varphi}\frac{|\nabla\psi|^2}{R^2},$$

$$g_{33} = R^2,$$

$$dl_\theta = dR\left[1+\left(\frac{\partial\psi}{\partial R}\Big/\frac{\partial\psi}{\partial Z}\right)^2\right]^{1/2} = dZ\left[1+\left(\frac{\partial\psi}{\partial Z}\Big/\frac{\partial\psi}{\partial R}\right)^2\right]^{1/2}.$$

The poloidal flux Ψ is defined by

$$\Psi = \int d\mathbf{S}_{\rm pol}\cdot\mathbf{B}_0 = \int d\varphi\int d\psi\,\frac{\partial\mathbf{x}}{\partial\varphi}\times\frac{\partial\mathbf{x}}{\partial\psi}\cdot\mathbf{B}_0$$

$$= 2\pi\int d\psi\; J_{\psi\theta\varphi}\frac{\partial\theta}{\partial\mathbf{x}}\cdot\mathbf{B}_0 = \int d\psi\frac{2\pi J_{\psi\theta\varphi}B_\theta}{|\partial\mathbf{x}/\partial\theta|},$$

in which ψ is an – up to now arbitrary – radial variable. If this radial coordinate ψ is identified with the poloidal flux Ψ, the integrand of the above integral should be 1 ($\Psi = \int d\Psi$), and so the poloidal magnetic field can be written as

$$B_\theta = \frac{1}{2\pi J_{\psi\theta\varphi}}\left|\frac{\partial\mathbf{x}}{\partial\theta}\right| = \frac{|\nabla\Psi|}{2\pi R} \qquad \left(\text{for any } \psi, \left|\frac{\partial\mathbf{x}}{\partial\theta}\right| = \sqrt{g_{22}} = \frac{J_{\psi\theta\varphi}|\nabla\psi|}{R}\right).$$

Consequently,

$$B_0 = \frac{1}{R}\left[\left(\frac{|\nabla\Psi|}{2\pi}\right)^2 + B^2_{\varphi m}R^2_m\right]^{1/2},$$

$$\cos\alpha = \frac{B_\varphi}{B_0}\left[1+\left(\frac{|\nabla\Psi|}{2\pi B_{\varphi m}R_m}\right)^2\right]^{-1/2},$$

$$\sin\alpha = \frac{B_\theta}{B_0}\left[1+\left(\frac{2\pi B_{\varphi m}R_m}{|\nabla\Psi|}\right)^2\right]^{-1/2}.$$

If another choice is made, the identity $\nabla\Psi = \nabla\Psi(\psi) = (d\Psi/d\psi)\nabla\psi$ is used. Defining the local safety factor in the usual manner as the variation of the toroidal angle with the poloidal angle along a magnetic field line,

$$q = \left.\frac{d\varphi}{d\theta}\right|_{\text{along}\mathbf{B}_0} = \frac{dl_\varphi}{dl_\theta}\frac{(g_{22})^{1/2}}{R} = \frac{B_\varphi}{B_\theta}\frac{(g_{22})^{1/2}}{R},$$

yields an expression relating the Jacobian and q:

$$J_{\psi\theta\varphi} = \frac{qR}{2\pi B_\varphi}.$$

This equality stresses that if one requires q to be a surface quantity ('the' safety factor, which unlike the above local q is independent of the choice of the poloidal angle), one cannot freely choose the poloidal angle. Conversely, choosing an arbitrary poloidal angle requires the local safety factor to satisfy the above relation

https://doi.org/10.1017/S0022377801001246 Published online by Cambridge University Press

with the Jacobian, so, unless $J_{\psi\theta\varphi}/R^2$ is a surface quantity, the local and average safety factors on the magnetic surface are not identical. The current I and the current density J_0 are related through

$$I(\Psi) = \frac{1}{\mu_0}\int d\mathbf{S}_{\rm tor}\cdot\boldsymbol{\nabla}\times\mathbf{B} = \frac{1}{\mu_0}\int d\theta\left|\frac{\partial\mathbf{x}}{\partial\theta}\right| B_\theta = \frac{1}{\mu_0 B_{\varphi m} R_m}\int d\theta\; q\left|\frac{\boldsymbol{\nabla}\Psi}{2\pi}\right|^2$$
$$= \frac{1}{2\pi\mu_0}\int d\theta\;\frac{J_{\psi\theta\varphi}}{R^2}|\boldsymbol{\nabla}\Psi|^2 = \int d\Psi\; J_0(\Psi)\int d\theta\frac{J_{\psi\theta\varphi}}{R}$$
$$\mathscr{J} = \mathscr{J}_0(\Psi)\mathbf{e}_\varphi, \qquad \mathscr{J}_0(\Psi) = \frac{dI(\Psi)}{d\Psi}\Big/\int d\theta\frac{J_{\psi\theta\varphi}}{R}.$$

For the particular choice $q = q(\Psi)$, the directional derivative along the magnetic field can be written as

$$\mathbf{e}_\parallel\cdot\boldsymbol{\nabla} = \frac{1}{2\pi B_0 J_{\psi\theta\varphi}}\left[\frac{\partial}{\partial\theta} + q(\Psi)\frac{\partial}{\partial\varphi}\right],$$

and the Doppler shift takes the simple form

$$k_\parallel v_\parallel = (m + nq)\dot{\theta},$$

in which

$$\dot{\theta} = \frac{d\theta}{dt} = \frac{v_\parallel\sin\alpha}{|\partial\mathbf{x}/\partial\theta|}, \qquad v_\parallel = v\left(1 - \frac{xB_0}{B_m}\right)^{1/2}.$$

It is advantageous to choose a coordinate system for which all geometric coefficients can easily be computed analytically. For the particular choice adopted here, originally proposed for the BRAYCOH ray-tracing code (Van Eester et al. 1985),

$$R = R_0 + \tilde{\Delta}_0\left[1 - \left(\frac{\rho}{a_p}\right)^2\right] + \rho\cos\theta + \frac{\delta\rho^2}{2a_p}(\cos 2\theta - 1),$$
$$Z = \kappa\rho\sin\theta,$$

the inverse transformation is available in explicit analytical form:

$$\rho = \frac{1}{|\beta|}\left[\tfrac{1}{2} - \tilde{\alpha}\beta - (\tfrac{1}{4} - \tilde{\alpha}\beta - \gamma\rho^2)^{1/2}\right]^{1/2}, \qquad \theta = \arcsin\left[\frac{Z}{\kappa\rho(R,Z)}\right],$$

with

$$\tilde{\alpha} = R - R_0 - \tilde{\Delta}_0 + \frac{\delta}{a_p}\left(\frac{Z}{\kappa}\right)^2, \qquad \beta = \frac{\tilde{\Delta}_0}{a_p^2}, \qquad \gamma = \left(\frac{Z}{\kappa}\right)^2,$$

so that analytical expressions for all geometric quantities can be found. One has, for example,

$$J_{\psi\theta\varphi} = \frac{\kappa\rho R\cos\theta}{\dfrac{d\psi}{d\rho}\dfrac{\partial\rho}{\partial R}},$$

$$\frac{\partial\rho}{\partial R} = \frac{\cos\theta}{1 - \dfrac{2\tilde{\Delta}_0\rho}{a_p^2}\cos\theta},$$

https://doi.org/10.1017/S0022377801001246 Published online by Cambridge University Press

$$\frac{\partial \rho}{\partial Z} = \frac{\sin\,\theta}{\kappa} \frac{1 + \dfrac{2\delta\rho}{a_p}\cos\,\theta}{1 - \dfrac{2\tilde{\Delta}_0\rho}{a_p^2}\cos\,\theta}.$$

In the above, the coordinate ρ is the half-width of the magnetic surface in the equatorial plane, $\tilde{\Delta}_0$ is the Shafranov shift of the magnetic axis, δ is the triangularity and κ is the elongation. The poloidal angle reduces to the usual one for magnetic surfaces with circular cross-section. If the angle between the toroidal and total magnetic fields is known at the reference position on the outboard side of the midplane, the radial derivative of the poloidal flux needed in the Jacobian can be evaluated by making use of $\boldsymbol{\nabla}\Psi = \boldsymbol{\nabla}\Psi(\rho) = (d\Psi/d\rho)\boldsymbol{\nabla}\rho$. One readily finds

$$\frac{d\Psi}{d\rho} = \frac{2\pi tg\alpha_m B_{0_\varphi}(R_m)R_m}{\boldsymbol{\nabla}\rho|_m} = \frac{2\pi tg\alpha_m B_{0_\varphi}(R_0)R_0}{\nabla\rho|_m}.$$

Conversely this expression allows one to find the poloidal field strength for a given current density profile.

Appendix B. Analytical expressions for circular orbits

When describing RF heating in tokamak geometry, finding the bounce-mode spectrum is a major task, since analytical expressions are usually not available for the nonlinear relation between the poloidal angle and the time that a guiding centre needs to arrive at that poloidal angle starting from the equatorial plane. For the case of a circular cross-section and when guiding centres are assumed to be confined to magnetic surfaces (i.e. when the toroidal angular momentum and the poloidal flux are confused), analytical espressions can be found for various bounce-averaged quantities (see Prudnikov et al. 1986). For passing particles ($2\tilde{\varepsilon}/(1+\tilde{\varepsilon}) \leqslant \xi_m^2 \leqslant 1$,

$$t(\theta) = \frac{2r}{|\sin\,\alpha|v}\left[\frac{1+\tilde{\varepsilon}}{(1-\tilde{\varepsilon})\xi_m^2}\right]^{1/2} \Pi(\varphi_{\rm pa}, \nu_{\rm pa}, k_{\rm pa}),$$

while for trapped particles ($0 \leqslant \xi_m^2 \leqslant 2\tilde{\varepsilon}/(1+\tilde{\varepsilon})$),

$$t(\theta) = \frac{2r}{|\sin\,\alpha|v}\left[\frac{1+\tilde{\varepsilon}}{2\tilde{\varepsilon}(1-\xi_m^2)}\right]^{1/2} \Pi(\varphi_{\rm tr}, \nu_{\rm tr}, k_{\rm tr}).$$

In these expressions, r is the magnetic surface on which the guiding-centre orbit lies, Π is the incomplete elliptic integral of the third kind,

$$\tilde{\varepsilon} = \frac{r}{R_0}, \qquad \xi_m = \frac{v_\parallel(\theta=0)}{v}, \qquad \nu_{\rm pa} = \frac{2\tilde{\varepsilon}}{\tilde{\varepsilon}-1}, \qquad \nu_{\rm tr} = \frac{1}{1-1/\xi_m^2}, \qquad k_{\rm pa}^2 = \frac{1}{k_{\rm tr}^2} = \frac{\nu_{\rm pa}}{\nu_{\rm tr}},$$

$$\varphi_{\rm pa} = \arcsin\left\{\left[\frac{(1-\cos\,\theta)(R_0/r-1)}{2(R_0/r+\cos\,\theta)}\right]^{1/2}\right\},$$

$$\varphi_{\rm tr} = \arcsin\left\{\left[\frac{(1-\cos\,\theta)(R_0/r+\cos\,\theta_{\rm max})}{(1-\cos\,\theta_{\rm max})(R_0/r+\cos\,\theta)}\right]^{1/2}\right\}.$$

From the above, half the transit time is easily found by letting $\theta = \pi$, i.e. $\varphi_{\rm pa} = \frac{1}{2}\pi$, for passing particles and $\theta = \theta_{\rm max}$, i.e. $\varphi_{\rm tr} = \frac{1}{2}\pi$, for trapped particles. For passing

https://doi.org/10.1017/S0022377801001246 Published online by Cambridge University Press

particles, the transit time is the bounce time, while for trapped particles, it is half the bounce time. The bounce average of $v_\parallel^2/v_\perp^2$ in the collision operator becomes

$$\left\langle \frac{v_\parallel^2}{v_\perp^2} \right\rangle = \frac{2r^2 \mathscr{H}}{vxt_{\text{transit}} \sin \alpha},$$

in which

$$\mathscr{H}_{\text{passing}} = \left[2 + (x-1)\frac{R_m}{r}\right]\left[\frac{R_0 - r}{R_m(1-x)}\right]^{1/2} \times \frac{\chi^2 E(k) + (k^2 - \chi^2)K(k) + (2\chi^2 - \chi^4 - k^2)\Pi(\chi^2, k)}{\chi^2(\chi^2 - 1)},$$

$$\mathscr{H}_{\text{trapped}} = \frac{R_m^2(1-x)/r^2}{[2xR_m/r]^{1/2}} \frac{\chi^2 E(k) + (k^2 - \chi^2)K(k) + (2k^2\chi^2 - \nu^4 - k^2)\Pi(\chi^2, k)}{\chi^2(k^2 - \chi^2)}.$$

Here, E, K and Π are elliptic integrals and

$$k_{\text{pa}}^2 = \frac{1}{k_{\text{tr}}^2} = \frac{2xr}{(1-x)(R_0 - r)}, \qquad \chi_{\text{pa}}^2 = \frac{2r}{(1-x)R_m}, \qquad \chi_{\text{tr}}^2 = 1 - \frac{1}{x}.$$

When the cross-section of the magnetic surface is not circular, the relation between the poloidal position and the time that a guiding centre needs to arrive at that position has to be evaluated numerically. Although the parallel velocity vanishes at the banana tips (which suggests that bounce integrals cannot easily be computed numerically, since the integrand diverges), the contribution from the region close to the bounce tips is negligible. For the transit time one has, for example, for vanishingly small ν

$$t_{\text{transit}} = 2\int_0^{\theta_{\max}} \frac{d\theta}{d\theta/dt} = 2\left(\int_0^{\theta_{\max}-\nu} \frac{d\theta}{d\theta/dt} + \int_{\theta_{\max}-\nu}^{\theta_{\max}} \frac{d\theta}{d\theta/dt}\right)$$

$$\approx 2\left[\text{const}\ \frac{\nu^{1/2}}{(\sin\ \theta_{\max})^{1/2}} + \int_{\theta_{\max}-\nu}^{\theta_{\max}} \frac{d\theta}{d\theta/dt}\right]$$

Only at the trapped/passing boundary (where the transit time goes to infinity; $\theta_{\max} = \pi$) is the contribution close to the banana tip not negligible.

References

Abramowitz, M. and Stegun, I. A. 1964 *Handbook of Mathematical Functions*. New York: Dover.

Bécoulet, A., Gambier, D. J. and Samain, A. 1991 *Phys. Fluids* **B3**, 137.

Bécoulet, A., Fraboulet, D., Giruzzi, G., Moreau, D., Saoutic, B. and Chinardet, J. 1994 *Phys. Plasmas* **1**, 2908.

Belikov, V. S. and Kolesnichenko, Y. I. 1982 *Plasma Phys.* **24**, 61.

Belikov, V. S. and Kolesnichenko, Y. I. 1994 *Plasma Phys. Contr. Fusion* **36**, 1703.

Bindslev, H., Woskow, P., Hoekzema, A., Machuzak, J., Porte, L. and Van Eester, D. 1999 In: *Proceedings of 26th EPS Conference on Controlled Fusion and Plasma Physics, Maastricht, 1999*. Mulhouse: EPS, p. 765.

Brambilla, M. 1999 *Plasma Phys. Contr. Fusion* **41**, 1.

Chang, C. S. and Colestock, P. 1990 *Phys. Fluids* **B2**, 310.

https://doi.org/10.1017/S0022377801001246 Published online by Cambridge University Press

Chang, C. S., Phillips, C. K., White, R., Zweben, S., Bonoli, P. T., Rice, J. E., Greenwald, M. J. and deGrassie, J. 1999 *Phys. Plasmas* **6**, 1969.

Colestock, P. L. and Kashuba, R. J. 1983 *Nucl. Fusion* **27**, 363.

Edery, D. and Picq, H 1986 *Comp. Phys. Commun.* **40**, 95.

Edery, D., Picq, H., Samain, A. and Gambier, D. J. 1987 Report EUR-CEA-FC 1334.

Eriksson, L.-G. and Helander, P. 1994 *Phys. Plasmas* **1**, 308.

Eriksson, L.-G., Hellsten, T. and Willen, U. 1993 *Nucl. Fusion* **7**, 1037.

Eriksson, L.-G., Mantsinen, M. J., Hellsten, T. and Carlsson, J. 1999 *Phys. Plasmas* **6**, 513.

Faulconer, D. W. and Liboff, R. L. 1972 *Phys. Fluids* **15**, 1831.

Gaffey, J. D. 1976 *J. Plasma Phys.* **16**, 149.

Gambier, D. J. and Samain, A. 1985 *Nucl. Fusion* **25**, 283.

Hamamatsu, K., Azumi, M., Kishimoto, Y., Fukuyama, A., Itoh, S.-I. and Itoh, K. 1989 *Nucl. Fusion* **29**, 147.

Hedin, J., Carlsson, J., Hellsten, T. and Jaun, A. 1998 *Plasma Phys. Contr. Fusion* **40**, 1085.

Hedin, J., Hellsten, T. and Carlsson, J. 1999 In: *Proceedings of Joint Varenna–Lausanne International Workshop on Theory of Fusion Plasmas, Varenna, 1998*. Bologna: ISPP-18 'Piero Caldirola', p. 467.

Hellsten, T., Carlsson, J. and Eriksson, L.-G. 1995 *Phys. Rev. Lett.* **74**, 3613.

Jaeger, E. F., Carter, M. D., Berry, L. A., Batchelor, D. B., Forest, C. B. and Weitzner, H. 1998 *Nucl. Fusion* **1**, 1.

Jaeger, E. F., Berry, L. A. D'Azevedo, E. F., Batchelor, D. B. and Carter, M. D. 2000 In: *Proceedings of Joint Varenna–Lausanne International Workshop on Theory of Fusion Plasmas, Varenna, 2000*. Bologna: ISPP-19 'Piero Caldirola', p. 45.

Karney, C. F. F. 1986 *Comp. Phys. Rep.* **4**, 183.

Kasilov, S. V., Pyatak, A. I. and Stepanov, K. N. 1990 *Nucl. Fusion* **30**, 2467.

Kaufman, A. N. 1972 *Phys. Fluids* **15**, 1063.

Kennel, C. F. and Engelmann, F. 1966 *Phys. Fluids* **9**, 2377.

Kupfer, K. 1991 In: *Proceedings of IAEA Technical Committee Meeting on Fast Wave Current Drive in Reactor Scale Tokamaks, Arles, 1991*. St Paul les Durance: CEA, p. 149.

Lamalle, P. U. 1993 *Phys. Lett.* **175A** 45.

Lamalle, P. U. 1994 Nonlocal theoretical generalization and tridimensional numerical study of the coupling of an ICRH antenna to a tokamak plasma. PhD Thesis, Université de Mons; LPP-ERM/KMS Laboratory Report 101.

Lamalle, P. U. 1997 *Plasma Phys. Contr. Fusion* **39**, 1409.

Lamalle, P. U. 1998 *Plasma Phys. Contr. Fusion* **40**, 465.

Louis, Y. 1995 Etude analytique et numérique de la réponse diélectrique non-locale d'un plasma de tokamak à une perturbation radiofréquence, tenant compte de la toroidicité et des effets de décorrelation. PhD Thesis, Université Libre de Bruxelles; LPP-ERM/KMS Laboratory Report 103.

O'Brien, M. R., Cox, M. and Start, D. F. H. 1986 *Nucl. Fusion* **26**, 1625.

Prudnikov, A. P., Brychkov, Y. A. and Marichev, O. I. 1986 *Integrals and Series*, Vol. I. New York: Gordon and Breach.

Sauter, O. and Václavík, J. 1992 *Nucl. Fusion* **32**, 1455.

Scharer, J., Jacquinot, J., Lallia, P. and Sand, P. 1985 *Nucl. Fusion* **25**, 435.

Stix, T. H. 1975 *Nucl. Fusion* **15**, 737.

Van Eester, D. 1995 *J. Plasma Phys.* **54**, 31.

Van Eester, D. 1998 *J. Plasma Phys.* **60**, 627.

Van Eester, D. 1999 *Plasma Phys. Contr. Fusion* **41**, L23.

Van Eester, D. and Koch R. 1998 *Plasma Phys. Contr. Fusion* **40**, 1949.

Van Eester, D., Bhatnagar, V. P. and Koch, R. 1985 *Plasma Phys. Contr. Fusion* **27**, 1015.

Van Eester, D., Louis, Y., Lamalle, P. U. and Koch, R. 1996 *Phys. Rev. Lett.* **218A**, 70.